Steady-state solutions in a three-dimensional nonlinear pool-boiling heat-transfer model

Michel Speetjens[*], Arnold Reusken[*†], Wolfgang Marquardt[‡]

RWTH Aachen, Templergraben 55, D-52056 Aachen, Germany.

Abstract

We consider a relatively simple model for pool-boiling processes. This model involves only the temperature distribution within the heater and describes the heat exchange with the boiling medium via a nonlinear boundary condition imposed on the fluid-heater interface. This results in a standard heat-transfer problem with a nonlinear Neumann boundary condition on part of the boundary. In a recent paper [1] we analysed this nonlinear heat-transfer problem for the case of *two space dimensions* and in particular studied the qualitative structure of steady-state solutions. The study revealed that, depending on system parameters, the model allows both multiple homogeneous and multiple heterogeneous temperature distributions on the fluid-heater interface. In the present paper we show that the analysis from Speetjens *et al.* [1] can be generalised to the physically more realistic case of *three space dimensions*. A fundamental shift-invariance property is derived that implies multiplicity of heterogeneous solutions. We present a numerical bifurcation analysis that demonstrates the multiple solution structure in this mathematical model by way of a representative case study.

Keywords: pool boiling, nonlinear heat transfer, bifurcations, numerical simulation

1 Introduction

Pool boiling refers to boiling processes that lean on natural convection as means for heat transfer through the boiling medium and is the key mode of thermal transport in many practical applications. Local heat-transfer phenomena near heating walls in industrial

[*]Chair of Numerical Analysis. This author was supported by the German Research Foundation through the Research Training Group "Hierarchy and Symmetry in Mathematical Models"

[†]Corresponding author: Chair of Numerical Analysis, RWTH Aachen, Templergraben 55, D-52056 Aachen, Germany, +49-241-80-97973, reusken@igpm.rwth-aachen.de

[‡]Chair of Process Systems Engineering

boiling equipment (e.g. evaporators and kettle reboilers) for instance are essentially pool-boiling processes [2]. Furthermore, pool boiling is emerging as novel cooling technique for electronics components [3]. Despite its importance, many aspects of (pool) boiling remain largely unexplored to date, mainly due to the immense complexity of the process induced by the intricate interplay between hydro- and thermodynamics. Studies on boiling known in the literature are mainly experimental and empirical. Theoretical investigations are scarce. The theoretical analysis presented in this paper is intended to contribute to a better understanding of fundamental phenomena in pool boiling.

In pool boiling there are three fundamental states, namely nucleate, transition and film boiling, that occur successively with increasing temperature [4]. Nucleate boiling is, as opposed to film boiling, an efficient and safe mode of heat transfer and the sought-after state in typical applications. Nucleate boiling transits into film boiling upon exceeding the so-called critical heat flux (CHF) through the intermediate state of transition boiling. This transition results in a dramatic increase in interface temperature due to the substantial drop in the heat-transfer coefficient when going from nucleate boiling (homogeneous liquid-like mixture) to film boiling (vapour blanket on the interface). This manifests itself in the essentially nonlinear relation between the mean heat flux and the mean fluid-heater interface temperature, i.e. the boiling curve [4]. Improvement of boiling processes involves finding a good balance between high efficiency (close to CHF) and low risk (safe distance from CHF). This requires an in-depth understanding of transition boiling [5].

Transition boiling may in a simplified description be considered as a state of "two-mode boiling" that consists of coexisting nucleate-boiling and film-boiling regions [6]. A more intricate – and most likely more precise – description of the two-phase structure in transition boiling has been derived by Auracher and co-workers (see [7] for a survey). Moreover, transition boiling is an inherently unstable state that naturally evolves towards one of the two stable boiling modes, i.e. nucleate or film boiling, unless actively stabilised through temperature control [8]. On mesoscopic length and time scales two-mode boiling states correspond to heterogeneous temperature fields on the interface: "lower" temperatures correspond to nucleate-boiling regions; "higher" temperatures are associated with film-boiling regions.[1] The propagation of boundaries between adjacent boiling regions during evolution of the transition mode towards one of the stable modes is consistent with the propagation of thermal waves at the fluid-heater interface [10]. This phenomenological connection between a (mesoscopic) boiling mode and interface temperature admits a heater-only modelling approach that leaves out the boiling medium and describes the (qualitative) behaviour of the boiling system entirely in terms of the temperature distribution within the heater. This leads to a *nonlinear heat-transfer model* in terms of which fundamental (mesoscopic) boiling phenomena can be analysed by means of numerical simulation.

The heater-only approach has found widespread application for the analysis of pool boiling on "thin" heaters (essentially wires and foils) [10–15]. In such thin configurations, which correspond to *spatially one-dimensional* (1D) models, the heat-flux relation leads to

[1] Here mesoscopic means locally averaged in space and time over intervals larger than bubble dimensions and bubble lifetimes in order to smooth out microscopic short-term fluctuations [9].

a source term in the governing equation, resulting in a reaction-diffusion-type model [16]. First extensions to finite-thickness heaters, using a *spatially two-dimensional* (2D) model, have been presented in [16].

The transition behaviour of the heater-only problem basically involves two issues: (i) formation and (ii) dynamics of heterogeneous temperature fields [7]. These two issues lead to questions concerning existence and stability of steady-state solutions. The present study concerns the issue of existence of steady-state solutions. An extensive analysis of the steady-state behaviour of a *spatially 2D* heater problem is presented in [1], based upon the model proposed in [16], which demonstrated multiple steady-state solutions for specific conditions. In the present study we generalise the 2D analysis [1] to the physically more realistic *spatially three-dimensional* (3D) pool-boiling problem. The solution strategy is similar to that used for the 2D study in [1]. We apply a numerical continuation algorithm combined with the method of separation-of-variables and a Fourier collocation method. However, if we extend this approach from the 2D to the 3D case this leads to a strong increase of the numerical complexity and consequently it becomes much more technical. The 2D analysis in [1] is based on univariate Fourier expansions; the 3D case requires bivariate Fourier series. The 2D problem admits only one-dimensional kernels for the Jacobian in the bifurcation analysis, whereas the 3D problem turns out to admit multi-dimensional kernels that lead to much complexer bifurcation behaviour. In [1] we give an extensive analysis in which many model parameters are varied and corresponding bifurcation diagrams are derived. In the 3D analysis presented in this paper, due to its greater complexity, only one case study is treated.

The paper is organised as follows. Section 2 introduces the 3D model problem. Section 3 discusses the analytical reduction of the 3D problem to a 2D reduced problem for the temperature on the fluid-heater interface. Key properties of this reduced model are derived. In Section 4 we treat the discretisation method and the continuation algorithm. In Section 5 this approach is applied to a representative case study. Conclusions are drawn in Section 6.

2 Mathematical model for pool boiling

Our pool boiling analysis is based on the heater-only modelling approach introduced in Section 1. We consider the three-dimensional rectangular heater $\mathcal{D} = [0, L] \times [0, W] \times [0, H]$, with boundary $\Gamma = \partial\mathcal{D} = \Gamma_H \cup \Gamma_A \cup \Gamma_F$ as a natural extension to the 2D configuration studied in [1]. The boundary segments are $\Gamma_H = \{(x, y, z) \in \mathcal{D} \mid z = 0\}$ (heat supply), $\Gamma_A = \big\{ (x, y, z) \in \mathcal{D} \mid x \in \{0, L\} \quad \text{or} \quad y \in \{0, W\} \big\}$ (adiabatic sidewalls) and $\Gamma_F = \{(x, y, z) \in \mathcal{D} \mid z = H\}$ (fluid-heater interface). The heat transfer is described in terms of the superheat T, i.e. the temperature excess beyond the boiling point. The steady-state temperature distribution $T(\boldsymbol{x})$ in $\mathcal{D}$ is governed by the heat equation

$$\Delta T = 0, \quad \lambda \frac{\partial T}{\partial n}|_{\Gamma_H} = \bar{q}_H, \quad -\lambda \tfrac{\partial T}{\partial n}|_{\Gamma_F} = \bar{q}_F(T_F), \quad \tfrac{\partial T}{\partial n}|_{\Gamma_A} = 0, \tag{1}$$

where T_F denotes the interface temperature on the boundary segment Γ_F. The constant λ is the thermal conductivity of the heater; $\bar{q}_H$ and $\bar{q}_F$ represent the constant heat supply

and temperature-dependent heat transfer to the boiling fluid, respectively.

Closure of the heat-transfer model requires specification of the heat-flux function $\bar{q}_F(T_F)$. Physical considerations suggest local heat-transfer coefficients specific to liquid and vapour contact for "lower" and "higher" local interface temperatures T_F, respectively. This implies that the function $\bar{q}_F(T_F)$ should be qualitatively similar to the global boiling curve. For simplicity, we identify $\bar{q}_F(T_F)$ with the functional form of the global boiling curve (Figure 1*a*). This boiling curve consist of three distinct regimes that each correspond to one of the boiling modes: nucleate boiling ($0 \leq T \leq T_C$); transition boiling ($T_C < T < T_M$); film boiling ($T \geq T_M$). The nucleate and film boiling regions represent local liquid and vapour contacts respectively; the transition region is modeled by a smooth connection between the different heat-transfer coefficients of adjacent liquid and vapour contacts. An explicit expression for $\bar{q}_F(T_F)$ is given below.

We formulate the heat-transfer problem (1) in non-dimensional form through rescaling of the variables: $\boldsymbol{x}' = \boldsymbol{x}/L$, $T' = T/T_D$, $q'_H = \bar{q}_H/Q_H$ and $q'_F = \bar{q}_F/Q_C$. Substitution into the governing equations and dropping primes yields the non-dimensional model

$$\Delta T = 0, \quad \Lambda \frac{\partial T}{\partial n}|_{\Gamma_H} = 1, \quad -\Lambda \tfrac{\partial T}{\partial n}|_{\Gamma_F} = \Pi_2\, q_F(T_F), \quad \tfrac{\partial T}{\partial n}|_{\Gamma_A} = 0, \tag{2}$$

on the non-dimensional heater $\mathcal{D} = [0,1] \times [0, D_1] \times [0, D_2]$, with system parameters

$$\Lambda = \frac{\lambda T_D}{Q_H L}, \;\; D_1 = \frac{W}{L}, \;\; D_2 = \frac{H}{L}, \;\; \Pi_1 = \frac{Q_C}{Q_M}, \;\; \Pi_2 = \frac{Q_C}{Q_H}, \;\; \Pi_3 = \frac{T_C}{T_M}. \tag{3}$$

Here Q_H is a fixed typical value for the heat supply; in the current case of a constant heat supply we use $Q_H = \bar{q}_H$ (i.e. $q'_H = 1$). Note that $q_F = \bar{q}_F/Q_C$ is the normalised boiling curve (i.e. rescaled with Q_C instead of Q_H). The latter can be parameterised by

$$q_F(T_F) = h(T_F)T_F, \quad h(T_F) := C_D \left\{F_1 - F_2 H(C_D T_F - 1)\right\}, \tag{4}$$

with $h(T_F)$ the heat-transfer coefficient and $H(\zeta) = \frac{1}{2}\left[\tanh\left(\frac{2\zeta}{W}\right) + 1\right]$ the smoothed Heaviside function. The parameter W sets the width of the transition region (from $H = 0$ to $H = 1$) around $\zeta = 0$ and is specified *a-priori*. Coefficients C_D and $F_{1,2}$ are fixed for given W and Π_1 following the procedure in [1]. Figure 1*b* shows q_F for $W = 1$ and $\Pi_1 = 4$. The present boiling curve is a generalisation of that proposed in [16] with the transition width W as additional parameter.

3 Analysis of the steady-state heat-transfer problem

The method of separation-of-variables [17] enables derivation of a (formal) solution of the Laplace equation and the linear Neumann conditions on Γ_H and Γ_A in (2). This results in

$$T(x,y,z) = \sum_{n,p=0}^{\infty} \widetilde{T}_{n,p} \cos(n\pi x) \cos\left(\frac{p\pi y}{D_1}\right) \frac{\cosh(\kappa_{n,p}\pi z)}{\cosh(\kappa_{n,p}\pi D_2)} + \frac{D_2 - z}{\Lambda}, \tag{5}$$

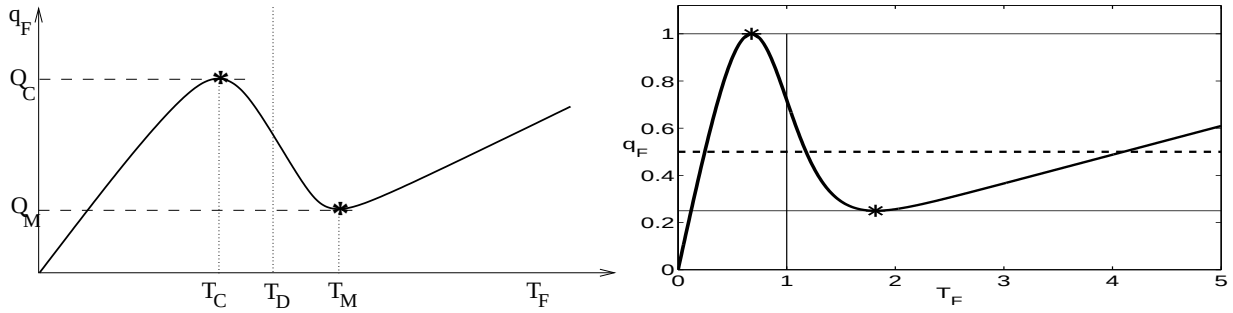

a) Global boiling curve. *b) Normalised boiling curve q_F.*

Figure 1: *Heat-flux function q_F. Panel a gives the global boiling curve. Temperatures T_C and T_M coincide with the extrema (stars); T_D is a typical temperature during transition boiling. Panel b gives the corresponding normalised boiling curve q_F for $\Pi_1 = 4$ and $W = 1$. $T = 1$ is the non-dimensional counterpart of T_D; the extrema (stars) correspond with $q_F = 1$ and $q_F = \Pi_1^{-1}$. The dashed line represents the normalised heat supply $\bar{q}_H/Q_C = \Pi_2^{-1}$.*

where $\kappa_{n,p} := \sqrt{n^2 + (p/D_1)^2}$. The coefficients $\widetilde{T}_{n,p}$ form the spectrum of the Fourier cosine expansion

$$T_F(x,y) := T(x,y,D_2) = \sum_{n,p=0}^{\infty} \widetilde{T}_{n,p} \cos(n\pi x) \cos\Big(\frac{p\pi y}{D_1}\Big), \tag{6}$$

of the interface temperature. The coefficients $\widetilde{T}_{n,p}$ are determined by the nonlinear Neumann boundary condition on Γ_F. Substitution of (5) into the nonlinear condition and using the relation $q_F(T_F) = h(T_F)T_F$ leads to

$$\sum_{n,p=0}^{\infty} \kappa_{n,p}\pi \tanh(\kappa_{n,p}\pi D_2)\widetilde{T}_{n,p} \cos(n\pi x) \cos\Big(\frac{p\pi y}{D_1}\Big) + \alpha(T_F(x,y))T_F(x,y) - \frac{1}{\Lambda} = 0, \tag{7}$$

for all $(x,y) \in \Gamma_F$, with

$$\alpha(T_F) = \frac{\Pi_2}{\Lambda} h(T_F) = \frac{\Pi_2}{\Lambda} \frac{q_F(T_F)}{T_F},$$

the scaled heat-transfer coefficient. *Thus the 3D problem* (2) *simplifies to the 2D reduced heat-transfer problem* (7) *involving only the temperature $T_F(x,y)$ on the boundary Γ_F.* The series in (6) and (7) are formal expressions; their convergence is discussed below.

We first consider the special case of *homogeneous* interface temperatures T_F, implying $T_F(x,y) = \widetilde{T}_{0,0}$ and $\widetilde{T}_{n,p} = 0$ for all $(n,p) \neq (0,0)$. The reduced problem (7) simplifies to

$$q_F(\widetilde{T}_{0,0}) = \Pi_2^{-1}, \tag{8}$$

and $\widetilde{T}_{0,0}$ coincides with the intersection(s) between boiling curve q_F and normalised heat-supply $\bar{q}_H/Q_C = \Pi_2^{-1}$ (dashed line in Figure 1*b*). From Figure 1*b* it follows that, depending

on the system parameters Π_1 and Π_2, we can have one, two or three solutions for $\widetilde{T}_{0,0}$. Note that in this homogeneous case the heat-transfer coefficient $h(T_F)$ is constant and thus the Neumann boundary condition on Γ_F is linear. The corresponding solution in $\mathcal{D}$ is given by

$$T(x,y,z) = \frac{D_2}{\Lambda}\left(1 - \frac{z}{D_2}\right) + \widetilde{T}_{0,0}\ , \tag{9}$$

i.e., a linear profile with constant interface temperature $T_F(x,y) = \widetilde{T}_{0,0}$ given by (8).

We now return to the general (heterogeneous) case and derive two important properties. To this end we introduce the spaces of *convergent* bivariate Fourier cosine series for $k, \ell \geq 1$:

$$V_{k,\ell} := \{\, g:\, \mathbb{R}^2 \to \mathbb{R} \mid g(x,y) = \sum_{n,p=0}^{\infty} a_{kn,\ell p} \cos(kn\pi x) \cos\left(\frac{\ell p \pi y}{D_1}\right)\ \ \forall\ (x,y) \in \mathbb{R}^2\,\}. \tag{10}$$

and spaces of *convergent* univariate Fourier cosine series:

$$V_{k,\infty} := \{\, g:\, \mathbb{R}^2 \to \mathbb{R} \mid g(x,y) = \sum_{n=0}^{\infty} a_{kn} \cos(kn\pi x) \quad \forall\ (x,y) \in \mathbb{R}^2\,\}, \quad k \geq 1,$$

$$V_{\infty,\ell} := \{\, g:\, \mathbb{R}^2 \to \mathbb{R} \mid g(x,y) = \sum_{p=0}^{\infty} a_{\ell p} \cos\left(\frac{\ell p \pi y}{D_1}\right) \quad \forall\ (x,y) \in \mathbb{R}^2\,\}, \quad \ell \geq 1.$$

Remark 1 For brevity we introduce one notation for the bivariate and univariate Fourier series. Univariate functions $g \in V_{k,\ell}$ with $k < \infty$, $\ell = \infty$ are represented as

$$g(x,y) = \sum_{n=0}^{\infty} a_{kn} \cos(kn\pi x) =: \sum_{n,p=0}^{\infty} a_{kn,\ell p} \cos(kn\pi x) \cos\left(\frac{\ell p \pi y}{D_1}\right), \tag{11}$$

with $a_{kn,\ell p} := 0$ for all $p \geq 1$, $a_{kn,\ell p} := a_{kn}$ for $p = 0$. Similarly for $\ell < \infty$, $k = \infty$.

Functions from the space $V_{k,\ell}$ are $\frac{2}{k}$-periodic in x, $\frac{2D_1}{\ell}$-periodic in y (with $\frac{c}{\infty}$-periodic:=constant) and even: $g(x,y) = g(-x,y) = g(x,-y)$. Such functions are uniquely determined by their values at $(x,y) \in [0, \frac{1}{k}] \times [0, \frac{D_1}{\ell}]$ (with $\frac{c}{\infty} := 0$). For $1 \leq k, \ell < \infty$, the inclusions $V_{\infty,\ell} \subset V_{2k,\ell} \subset V_{k,\ell}$, $V_{k,\infty} \subset V_{k,2\ell} \subset V_{k,\ell}$ and $V_{k,\ell} \subset V_{1,1}$ hold. The Fourier transform on $V_{1,1}$ is denoted by $\mathcal{F} : V_{1,1} \to \mathbb{R}^{\infty\times\infty}$:

$$\text{for}\ \ g(x,y) = \sum_{n,p=0}^{\infty} a_{n,p} \cos(n\pi x) \cos\left(\frac{p\pi y}{D_1}\right), \quad \mathcal{F}(g) := (a_{n,p})_{n,p=0}^{\infty}. \tag{12}$$

Here $\mathbb{R}^{\infty\times\infty}$ denotes the space of infinite matrices with real entries. For $\mathbf{b} := (b_{n,p})_{n,p=0}^{\infty}$, $\mathbf{c} := (c_{n,p})_{n,p=0}^{\infty} \in \mathbb{R}^{\infty\times\infty}$ we define the Hadamard product $\mathbf{b} * \mathbf{c} := (b_{n,p}c_{n,p})_{n,p=0}^{\infty}$, i.e., elementwise multiplication of the entries in the matrices. In view of (7) we introduce the infinite matrix $\mathbf{d} = (d_{n,p})_{n,p=0}^{\infty}$ defined by

$$d_{n,p} := \kappa_{n,p}\pi \tanh(\kappa_{n,p}\pi D_2) \quad \text{for all}\ \ n,p \geq 0. \tag{13}$$

To guarantee that the expressions on the left-hand side in (7) are well-defined we only consider functions from the following subset of $V_{1,1}$:

$$S := \{\, g \in V_{1,1} \mid \mathbf{d} * \mathcal{F}(g) \in \mathrm{range}(\mathcal{F}) \ \text{ and } \ (\alpha \circ g)g \in V_{1,1} \,\}.$$

Remark 2 *Sufficiently smooth* functions $g \in V_{1,1}$ are elements of S. We do not study this smoothness issue here. In our numerical simulations we always observed that the discrete solutions show exponential convergence to very smooth continuous functions that lie in S.

The operator on the left-hand side in (7) has the following form

$$\mathcal{G}(T_F) := \mathcal{F}^{-1}\big(\mathbf{d} * \mathcal{F}(T_F)\big) + (\alpha \circ T_F)T_F - \frac{1}{\Lambda}, \quad \text{for } \ T_F \in S. \tag{14}$$

From the definition of S it immediately follows that $\mathcal{G} : S \to V_{1,1}$. Thus (7) leads to the following problem:

$$\text{Determine } T_F \in S \text{ such that } \quad \mathcal{G}(T_F) = 0\,. \tag{15}$$

The operator $\mathcal{G}$, defined on S, is (strongly) nonlinear. Homogeneous solutions (8) satisfy $\mathcal{G}(\widetilde{T}_{0,0}) = 0$. Below we show that for all $k, \ell \geq 1$ the range of $\mathcal{G}_{|V_{k,\ell}}$ is contained in $V_{k,\ell}$. This results in an important conservation-of-symmetry property in the continuation method.

Theorem 1 *The following holds:*

$$\mathcal{G} : V_{k,\ell} \cap S \to V_{k,\ell} \quad \textit{for all} \ \ k, \ell \geq 1.$$

The proofs of this theorem and of Theorem 2 are based on similar ideas as used in the analysis of the 2D problem in [1]. For completeness these proofs are given in the appendix. The next theorem yields a fundamental non-uniqueness result for heterogeneous solutions. For $\ell = \infty$ we use the notation as in Remark 1 and set $\frac{c}{\ell} := 0$, similarly for $k = \infty$.

Theorem 2 *Assume that there exist* $1 \leq k, \ell \leq \infty$ *and* $T_F \in V_{k,\ell} \cap S$ *such that* $T_F \notin V_{k',\ell}$ *for* $k' > k$, $T_F \notin V_{k,\ell'}$ *for* $\ell' > \ell$, *and*

$$T_F(x,y) = \sum_{n,p=0}^{\infty} \widetilde{T}_{kn,\ell p} \cos(kn\pi x) \cos\Big(\frac{\ell p \pi y}{D_1}\Big), \tag{16}$$

satisfies $\mathcal{G}(T_F) = 0$. *Define*

$$T_F^{*,1}(x,y) := T_F(x + \frac{1}{k}, y) = \sum_{n,p=0}^{\infty} \widetilde{T}^{(1)}_{kn,\ell p} \cos(kn\pi x) \cos\Big(\frac{\ell p \pi y}{D_1}\Big), \tag{17}$$

$$T_F^{*,2}(x,y) := T_F(x, y + \frac{D_1}{\ell}) = \sum_{n,p=0}^{\infty} \widetilde{T}^{(2)}_{kn,\ell p} \cos(kn\pi x) \cos\Big(\frac{\ell p \pi y}{D_1}\Big), \tag{18}$$

$$T_F^{*,3}(x,y) := T_F(x + \frac{1}{k}, y + \frac{D_1}{\ell}) = \sum_{n,p=0}^{\infty} \widetilde{T}^{(3)}_{kn,\ell p} \cos(kn\pi x) \cos\Big(\frac{\ell p \pi y}{D_1}\Big), \tag{19}$$

with

$$\widetilde{T}^{(1)}_{kn,\ell p} = (-1)^n \widetilde{T}_{kn,\ell p}, \quad \widetilde{T}^{(2)}_{kn,\ell p} = (-1)^p \widetilde{T}_{kn,\ell p}, \quad \widetilde{T}^{(3)}_{kn,\ell p} = (-1)^{n+p} \widetilde{T}_{kn,\ell p}. \tag{20}$$

Then $T_F^{*,i} \in V_{k,\ell} \cap S$ *satisfies* $\mathcal{G}(T_F^{*,i}) = 0$ *for* $i = 1, 2, 3$. *Furthermore* $T_F^{*,i} \neq T_F$ *holds for* $i = 1$ *or* 2.

Theorem 2 shows that heterogeneous solutions in $V_{1,1} \cap S$, if they exist, always induce three associated solutions, which we call *dual-shifted* solutions. At least one of these three, namely (17) or (18) (which may be equal), differs from T_F. This implies a fundamental non-uniqueness in the steady states under heterogeneous boiling conditions, consistent with laboratory experiments [7]. Note that the dual-shifted solutions $T_F^{*,i}$ are obtained from T_F by a translation with half the period of T_F. This implies certain symmetry relations between T_F and its dual-shifted solutions.

In the proof of Theorem 2 (appendix) we derive the following fundamental property of the operator $\mathcal{G} : V_{k,\ell} \cap S \to V_{k,\ell}$. For $i = 1, 2, 3$, let $s_i : \mathbb{R}^2 \to \mathbb{R}^2$ be the linear shift function $s_1(x, y) := (x + \frac{1}{k}, y)$, $s_2(x, y) := (x, y + \frac{D_1}{\ell})$, $s_3(x, y) := (x + \frac{1}{k}, y + \frac{D_1}{\ell})$. Note that $s_3 = s_1 \circ s_2 = s_2 \circ s_1$. For $T_F \in V_{k,\ell} \cap S$ the relations

$$\mathcal{G}(T_F \circ s_i) = s_i \circ \mathcal{G}(T_F), \quad i = 1, 2, 3, \tag{21}$$

hold. The relation for $i = 3$ is a direct consequence of the relations for $i = 1, 2$. Due to this commutator property of the nonlinear operator $\mathcal{G}$ and the linear shift operators s_i we obtain the non-uniqueness result in Theorem 2.

Remark 3 The particular form of the function $\alpha(\cdot)$ is not used the proofs of Theorem 1 and Theorem 2. These results hold for an arbitrary (smooth) boiling curves q_F.

In case of a square fluid-heater interface ($D_1 = 1$) a further multiplicity property holds:

Lemma 1 *Assume* $D_1 = 1$ *(square fluid-heater interface). Let* $T_F \in V_{k,\ell} \cap S$ *be a solution to the reduced heat-transfer problem:* $\mathcal{G}(T_F) = 0$. *Then there exists a dual-reflected solution* $T'_F(x, y) := T_F(y, x)$ *(with* $\widetilde{T}'_{kn,\ell p} = \widetilde{T}_{\ell p,kn}$*) that also satisfies the reduced heat-transfer problem:* $\mathcal{G}(T'_F) = 0$.

A proof of this result can be given using arguments as in the proof of Theorem 2.

4 Numerical solution method

The steady-state solutions follow from the characteristic equation (7). For homogeneous solutions the latter simplifies to (8) and can be solved by a standard root-finding algorithm. Thus homogeneous solution branches are readily identified. Heterogeneous solutions, on the other hand, have to be determined via the discretisation and continuation approach elaborated hereafter. Numerical results thus obtained will be presented in Section 5.

Discretisation of (7) is based on a standard Fourier collocation method [18]. We briefly review a few basic facts from discrete Fourier analysis. Consider for $N \in \mathbb{N}$ the equidistant mesh $x_j = j/N$, $j \in \mathbb{N}$. The discrete Fourier cosine transform of an even 2-periodic function $u(x) = u(x+2)$ is given by

$$u(x) = \sum_{n=0}^{N} \widetilde{u}_n \cos(n\pi x), \quad \widetilde{u}_n := \frac{c_n}{N}\Big\{u(0) + 2\sum_{j=1}^{N-1} u(x_j)\cos(n\pi x_j) + (-1)^n u(1)\Big\}, \tag{22}$$

with $c_0 = c_N = 1/2$ and $c_n = 1$ otherwise. This function satisfies

$$u(x_i) = \sum_{n=0}^{N} \widetilde{u}_n \cos(n\pi x_i) \quad \text{for all} \;\; 0 \le i \le N.$$

Hence, the (physical) values $\boldsymbol{u} = (u_0, \ldots, u_N)^T$, with $u_j := u(x_j)$, relate to the spectral coefficients $\widetilde{\boldsymbol{u}} = (\widetilde{u}_0, \ldots, \widetilde{u}_N)^T$ via

$$\boldsymbol{u} = \boldsymbol{V}_N \widetilde{\boldsymbol{u}}, \quad \boldsymbol{V}_N = (V_{ij})_{0\le i,j\le N}, \quad V_{ij} := \cos(j\pi x_i). \tag{23}$$

An elementary computation yields

$$(\mathbf{V}_N \boldsymbol{D})^{-1} = \frac{2}{N}\,\mathbf{V}_N \boldsymbol{D}, \quad \text{with} \;\; \boldsymbol{D} = \mathrm{diag}(1/2, 1, \ldots, 1, 1/2). \tag{24}$$

The above 1D Fourier representation of $u(x)$ readily extends to a 2D periodic function $u(x,y) = u(x+2, y+2D_1)$. We introduce the mesh $(x_i, y_j) := \big(\frac{i}{N}, \frac{jD_1}{P}\big)$, with $i = 0, \ldots, N$, $j = 0, \ldots, P$ and $N, P \in \mathbb{N}$. The truncated 2D Fourier cosine expansion of u is given by

$$u(x,y) \;\; = \;\; \sum_{n=0}^{N}\sum_{p=0}^{P} \widetilde{u}_{n,p} \cos(n\pi x)\cos\left(\frac{p\pi y}{D_1}\right). \tag{25}$$

and approximates the infinite Fourier expansion of functions $g(x,y) \in V_{1,1}$, cf. (10). The Fourier coefficients $\tilde{u}_{n,p}$ in (25) are uniquely determined by the equations

$$u(x_i, y_j) = \sum_{n=0}^{N}\sum_{p=0}^{P} \widetilde{u}_{n,p} \cos(n\pi x_i)\cos\left(\frac{p\pi y_j}{D_1}\right), \quad 0 \le i \le N,\, 0 \le j \le P. \tag{26}$$

Let $\boldsymbol{U} \in \mathbb{R}^{(N+1)\times(P+1)}$ be the matrix with entries $u_{i,j} = u(x_i, y_j)$ (physical values) and $\tilde{\boldsymbol{U}} \in \mathbb{R}^{(N+1)\times(P+1)}$ the matrix with Fourier coefficients $\tilde{u}_{n,p}$. Let $\mathbf{V}_P$ be the $(P+1)\times(P+1)$-matrix as in (23) but with $n\pi x_i$ replaced by $\frac{p\pi y_j}{D_1}$ $(0 \le p, j \le P)$. Thus we obtain

$$\boldsymbol{U} = \mathbf{V}_N\, \widetilde{\boldsymbol{U}}\, \mathbf{V}_P^T, \quad \widetilde{\boldsymbol{U}} = \mathbf{V}_N^{-1}\, \boldsymbol{U}\, \mathbf{V}_P^{-T}, \tag{27}$$

as matrix representation of (26). Due to orthogonality the inverses follow explicitly from (24). This yields the discrete Fourier transform $\boldsymbol{\mathcal{F}} : \mathbb{R}^{N\times P} \to \mathbb{R}^{N\times P}$:

$$\boldsymbol{\mathcal{F}}(\boldsymbol{U}) = \boldsymbol{V}_N^{-1}\boldsymbol{U}\boldsymbol{V}_P^{-T}, \quad \boldsymbol{\mathcal{F}}^{-1}(\widetilde{\boldsymbol{U}}) = \boldsymbol{V}_N\widetilde{\boldsymbol{U}}\boldsymbol{V}_P^T, \tag{28}$$

as discrete counterpart of the continuous Fourier transform (12).

The discretisation of the characteristic equation (7) is as follows: determine $T_F(x_i, y_j) = \sum_{n=0}^{N}\sum_{p=0}^{P}\widetilde{T}_{n,p}\cos(n\pi x_i)\cos\left(\frac{p\pi y_j}{D_1}\right)$, $0 \le i \le N$, $0 \le j \le P$, such that

$$\sum_{n=0}^{N}\sum_{p=0}^{P} d_{n,p}\widetilde{T}_{n,p}\cos(n\pi x_i)\cos\left(\frac{p\pi y_j}{D_1}\right) + \alpha(T_F(x_i,y_j))T_F(x_i,y_j) - \frac{1}{\Lambda} = 0, \tag{29}$$

for all $0 \le i \le N$, $0 \le j \le P$. Matrix notation enables a more compact form. To this end we define the $(N+1)\times(P+1)$ matrices $(\boldsymbol{T}_F)_{i,j} = T_F(x_i, y_j)$, $\big(\boldsymbol{M}(\boldsymbol{T}_F)\big)_{i,j} = \alpha(T_F(x_i,y_j))$ and $\boldsymbol{G}_{i,j} = 1/\Lambda$, for $0 \le i \le N$, $0 \le j \le P$, and $\boldsymbol{D}_{n,p} = d_{n,p}$, $(\tilde{\boldsymbol{T}}_F)_{n,p} = \tilde{T}_{n,p}$, for $0 \le n \le N$, $0 \le p \le P$. Furthermore, for matrices $\boldsymbol{A} = (a_{i,j})$, $\boldsymbol{B} = (b_{i,j})$ we define the Hadamard product $\boldsymbol{A} * \boldsymbol{B} = (c_{i,j})$ with $c_{i,j} := a_{i,j}b_{i,j}$. Using this notation the discrete problem (29) can be formulated as follows: determine $\boldsymbol{T}_F \in \mathbb{R}^{(N+1)\times(P+1)}$ such that

$$\boldsymbol{\mathcal{G}}(\boldsymbol{T}_F) := \boldsymbol{\mathcal{F}}^{-1}\big(\boldsymbol{D} * \boldsymbol{\mathcal{F}}(\boldsymbol{T}_F)\big) + \boldsymbol{M}(\boldsymbol{T}_F) * \boldsymbol{T}_F - \boldsymbol{G} = \boldsymbol{0}. \tag{30}$$

This is a nonlinear system in the (physical) unknown $\boldsymbol{T}_F$. (Note the similarity to (14)–(15).) The equivalent representation in the (spectral) unknown $\tilde{\boldsymbol{T}}_F$ is given by

$$\boldsymbol{D} * \tilde{\boldsymbol{T}}_F + \boldsymbol{\mathcal{F}}\big(\boldsymbol{M}(\boldsymbol{\mathcal{F}}^{-1}(\tilde{\boldsymbol{T}}_F)) * \boldsymbol{\mathcal{F}}^{-1}(\tilde{\boldsymbol{T}}_F)\big) - \tilde{\boldsymbol{G}} = \boldsymbol{0}, \quad \text{with } \tilde{\boldsymbol{G}} := \boldsymbol{\mathcal{F}}(\boldsymbol{G}). \tag{31}$$

The nonlinearity of (30) and (31) is due to the terms $\boldsymbol{M}(\boldsymbol{T}_F) * \boldsymbol{T}_F$ and $\boldsymbol{\mathcal{F}}\big(\boldsymbol{M}(\boldsymbol{\mathcal{F}}^{-1}(\tilde{\boldsymbol{T}}_F)) * \boldsymbol{\mathcal{F}}^{-1}(\tilde{\boldsymbol{T}}_F)\big)$, respectively. The former has a much simpler structure and admits a more efficient numerical treatment. Thus our numerical simulations are based on (30).

The discrete nonlinear system (30) is solved by a continuation method. Its nonlinearity stems entirely from the nonlinear heat-flux relation q_F according to (4). The system is linear if q_F is a linear function of T_F. This motivates the introduction of the non-physical nonlinearity parameter λ below as additional continuation parameter. We define

$$q_F(T_F, \lambda) := C_D\left\{F_1 - \lambda F_2 H(C_D T_F - 1)\right\} T_F, \quad \text{for } 0 \le \lambda \le 1. \tag{32}$$

For $\lambda = 0$ we have a linear boundary condition; for $\lambda = 1$ the actual nonlinear condition is recovered. Figure 2 illustrates the smooth transition of the boiling curve $q_F(T_F, \lambda)$ from the linear state ($\lambda = 0$) to the final nonlinear state ($\lambda = 1$) in Figure 1*b*.

The λ-dependent discrete nonlinear problem (30) can be represented as

$$\boldsymbol{\mathcal{G}}(\boldsymbol{T_F}, \lambda) := \boldsymbol{\mathcal{F}}^{-1}\big(\boldsymbol{D} * \boldsymbol{\mathcal{F}}(\boldsymbol{T}_F)\big) + \boldsymbol{M}_\lambda(\boldsymbol{T}_F) * \boldsymbol{T}_F - \boldsymbol{G} = \boldsymbol{0}, \tag{33}$$

where the λ-dependence enters the system via $\alpha_\lambda(T_F) = \frac{\Pi_2}{\Lambda}\frac{q_F(T_F,\lambda)}{T_F}$ in $\boldsymbol{M}_\lambda(\boldsymbol{T}_F)$. For each $\lambda \in [0,1]$ the set of *homogeneous* solutions (i.e. $\boldsymbol{T}_F$ = constant) of this system can be readily computed. Starting on a branch of homogeneous solutions we apply a continuation algorithm[2] to $\lambda \to \boldsymbol{\mathcal{G}}(\boldsymbol{T}_F, \lambda) = \boldsymbol{0}$ and determine bifurcations points on the homogeneous branches from which branches of heterogeneous solutions originate. This strategy is used in the numerical simulations in the next section.

[2]Here an in-house algorithm of the Chair of Process Systems Engineering, RWTH Aachen, has been used, based upon techniques described in [20]. Elaboration on this algorithm is beyond the present scope.

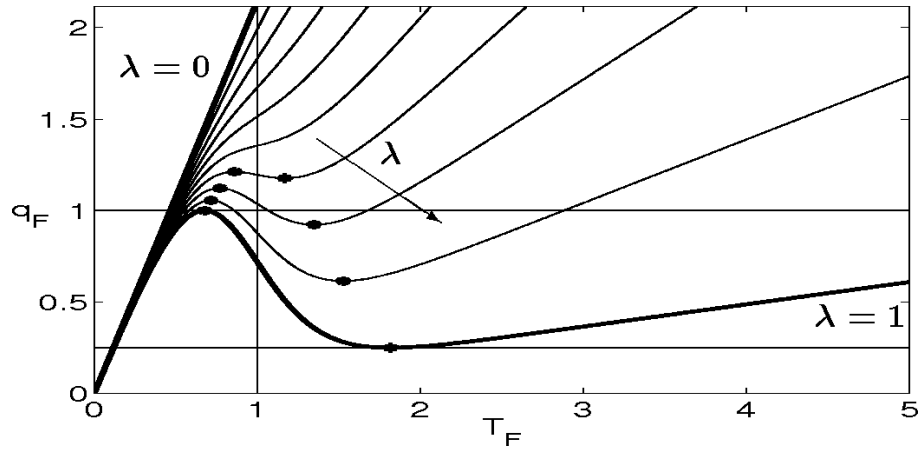

Figure 2: *Controlling the degree of nonlinearity of the boiling curve via the nonlinearity parameter λ. Shown is the smooth transition from a linear profile ($\lambda = 0$) towards the physical boiling curve (heavy; $\lambda = 1$) with increasing λ (arrow). The stars are the local maximum and minimum that occur for λ beyond some non-zero lower limit.*

5 Numerical experiments: a representative case study

We consider the discrete steady-state problem for fixed parameters: $\Lambda = 0.2$, $D_1 = 1$ (square interface), $D_2 = 0.2$, $\Pi_1 = 4$, $\Pi_2 = 2$ and $W = 1$. The steady-state solutions are determined with the approach introduced above. Homogeneous solutions are obtained by means of a standard Newton-type root-finding algorithm applied to (8); heterogeneous solutions follow from continuation of the nonlinear system (33) in the nonlinearity parameter λ. Important to note is that for smooth boiling curves (i.e. $W > 0$) the truncated Fourier expansion that underlies (33) exhibits exponential convergence. Hence, the continuation algorithm yields highly-accurate approximations to the continuous solution at any position $(x, y) \in \Gamma_F$ for moderate values of N and P. Here $(N, P) = (36, 36)$ has been used.

5.1 Homogeneous solutions

The homogeneous steady-state solutions (9) are uniquely determined by the constant interface temperature T_F as in (8). The latter is given by the (multiple) intersection(s) of the boiling curve with the normalised heat supply $\bar{q}_H/Q_C = \Pi_2^{-1}$ (Figure 1*b*). To determine the physically-meaningful homogeneous solutions it is sufficient to solve (8) for $\lambda = 1$. However, for bifurcation points on homogeneous branches that induce heterogeneous solution branches we need the homogeneous branches in the entire range $0 \leq \lambda \leq 1$. These branches readily follow from solving (8) in this λ-range. Two essentially different situations can be distinguished: (i) one solution $T_F^{(1)}$ for $0 \leq \lambda < \lambda_*$ (Figure 3*a*); (ii) three solutions $(T_F^{(1)}, T_F^{(2)}, T_F^{(3)})$ for $\lambda_* < \lambda \leq 1$ (Figure 3*c*). Both situations are connected through the degenerate case $\lambda = \lambda_*$, for which the local minimum of the boiling curve $q_F(\cdot, \lambda_*)$ touches the normalised heat supply $\bar{q}_H/Q_C = \Pi_2^{-1}$, causing the second and third solutions to co-

incide (Figure 3*b*). Thus the system undergoes a qualitative change at $\lambda = \lambda_*$ through a so-called tangent bifurcation [21].

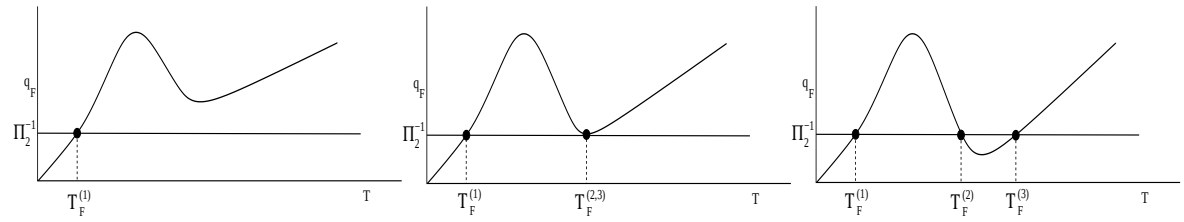

a) $\lambda < \lambda_*$ *b)* $\lambda = \lambda_*$ *c)* $\lambda > \lambda_*$

Figure 3: *Homogeneous solutions of the nonlinear system as a function of the nonlinearity parameter* λ*. Transition from the single-solution state (panel a) to the triple-solution state (panel c) takes place via the tangent bifurcation at* $\lambda = \lambda_*$ *(panel b).*

The homogeneous solutions as a function of the nonlinearity parameter λ are shown in the bifurcation diagram in Figure 5*b*. Solutions are represented by the functional $T_\Sigma = \sum_{n,p} \widetilde{T}_{n,p}$. The lower branch corresponds to $T_F^{(1)}$ that exists for all $0 \le \lambda \le 1$; the upper branch, with turning point at λ_* (circle), coincides with the two solutions $T_F^{(2,3)}$ that exist only in the interval $\lambda_* \le \lambda \le 1$ (here $\lambda_* \approx 0.926$). The lower and upper legs of this upper branch (connecting at a turning point) correspond with $T_F^{(2)}$ and $T_F^{(3)}$, respectively.

5.2 Bifurcation points on branches of homogeneous solutions

Multiple (heterogeneous) solutions emerge through bifurcations of the function $\lambda \to \boldsymbol{T}_F(\lambda)$, where $\boldsymbol{T}_F(\lambda)$ is a homogeneous solution of $\boldsymbol{\mathcal{G}}(\boldsymbol{T}_F, \lambda) = \boldsymbol{0}$. Bifurcations occur at λ-values for which the Jacobian of $\boldsymbol{\mathcal{G}}$ with respect to $\boldsymbol{T}_F$ is singular [20]. This Jacobian is given by

$$\boldsymbol{J} = \frac{\partial \boldsymbol{\mathcal{G}}(\boldsymbol{T}_F, \lambda)}{\partial \boldsymbol{T}_F}, \quad \boldsymbol{J}: \ \boldsymbol{W} \to \boldsymbol{\mathcal{F}}^{-1}\big(\boldsymbol{D} * \boldsymbol{\mathcal{F}}(\boldsymbol{W})\big) + \boldsymbol{Q}(\boldsymbol{T}_F, \lambda) * \boldsymbol{W}, \tag{34}$$

with $(\boldsymbol{Q}(\boldsymbol{T}_F, \lambda))_{i,j} = \frac{\Pi_2}{\Lambda} \frac{\partial q_F(T_F, \lambda)}{\partial T_F} =: \gamma((T_F)_{i,j}, \lambda)$ for $0 \le i \le N$, $0 \le j \le P$. On a homogeneous branch we have $\boldsymbol{T}_F = T_F \boldsymbol{1}$, with $\boldsymbol{1} \in \mathbb{R}^{(N+1)\times(P+1)}$ and $(\boldsymbol{1})_{i,j} = 1$ for $0 \le i \le N$, $0 \le j \le P$, and T_F the homogeneous interface temperature. This implies $\boldsymbol{Q}(\boldsymbol{T}_F, \lambda) = \gamma(T_F, \lambda)\boldsymbol{1}$ and thus on a homogeneous branch the Jacobian simplifies to

$$\boldsymbol{J}\big(\boldsymbol{W}\big) = \boldsymbol{\mathcal{F}}^{-1}\big(\boldsymbol{D} * \boldsymbol{\mathcal{F}}(\boldsymbol{W})\big) + \gamma(T_F, \lambda)\boldsymbol{W} = \boldsymbol{\mathcal{F}}^{-1}\left\{(\boldsymbol{D} + \gamma(T_F, \lambda)\boldsymbol{1}) * \boldsymbol{\mathcal{F}}(\boldsymbol{W})\right\}. \tag{35}$$

The Jacobian $\boldsymbol{J}$ is singular iff there exists a $\boldsymbol{W} \neq \boldsymbol{0}$ such that $\boldsymbol{J}(\boldsymbol{W}) = \boldsymbol{0}$. For the Jacobian in (35) this is equivalent to $(\boldsymbol{D} + \gamma(T_F, \lambda)\boldsymbol{1}) * \widetilde{\boldsymbol{W}} = \boldsymbol{0}$ for $\widetilde{\boldsymbol{W}} \neq \boldsymbol{0}$, with $\widetilde{\boldsymbol{W}} = \boldsymbol{\mathcal{F}}(\boldsymbol{W})$, which, in turn, is equivalent to

$$\zeta_{n,p}\widetilde{W}_{n,p} = 0 \quad \forall n, p, \quad \zeta_{n,p} := d_{n,p} + \gamma(T_F, \lambda), \tag{36}$$

with $\widetilde{W}_{n,p}$ the spectrum of $\boldsymbol{W}$ and $d_{n,p}$ as in (13). Non-zero $\widetilde{\boldsymbol{W}}$ requires $\widetilde{W}_{n,p} \neq 0$ and $\zeta_{n,p} = 0$ for at least one wave-number pair (n, p). This implies that non-trivial solutions $\boldsymbol{W}$ of $\boldsymbol{J}(\boldsymbol{W}) = \boldsymbol{0}$ are of the form

$$\boldsymbol{W} = \sum_{i=1}^{m} \widetilde{W}_{n_i,p_i} \boldsymbol{v}_{N,n_i} \boldsymbol{v}_{P,p_i}^T, \quad \text{with } (n_i, p_i) \text{ such that } \zeta_{n_i,p_i} = 0,\ 1 \leq i \leq m. \tag{37}$$

Here $\boldsymbol{v}_{N,r}$ ($\boldsymbol{v}_{P,r}$) denotes the r-th column of the matrix $\boldsymbol{V}_N$ ($\boldsymbol{V}_P$) and m is the number of vanishing coefficients $\zeta_{n,p}$, $0 \leq n \leq N, 0 \leq p \leq P$. Null solutions (37) are linear combinations of the m Fourier modes $\boldsymbol{v}_{N,n}\boldsymbol{v}_{P,p}^T$ that correspond with vanishing coefficients $\zeta_{n,p}$; the associated bifurcation (point) is called an "m-mode bifurcation". The coefficients $\widetilde{W}_{n_i,p_i}$ are free, implying that null solutions span an m-dimensional nullspace with Fourier modes as basis vectors, cf. (37). Because $d_{n,p} \geq 0$ for all $n, p \geq 0$, vanishing coefficients $\zeta_{n,p}$ require $\gamma(T_F, \lambda) < 0$ and thus a bifurcation on a homogeneous solution branch can only occur for those T_F for which the boiling curve has a negative slope ($\dot{q}_F \leq 0$). From Figure 3 it follows that only intersection $T_F^{(2)}$ meets this criterion, which implies that bifurcations are restricted to the $T_F^{(2)}$-branch in the bifurcation diagram (Figure 5*b*). This results in the fundamental property that *bifurcations – and thus multiple (heterogeneous) solutions – are essentially a transition phenomenon.* Figure 4*a* displays γ (heavy curve) as a function of λ on the $T_F^{(2)}$-branch together with $-d_{n,p}$ (dashed lines) for $p = 0$ and various n.

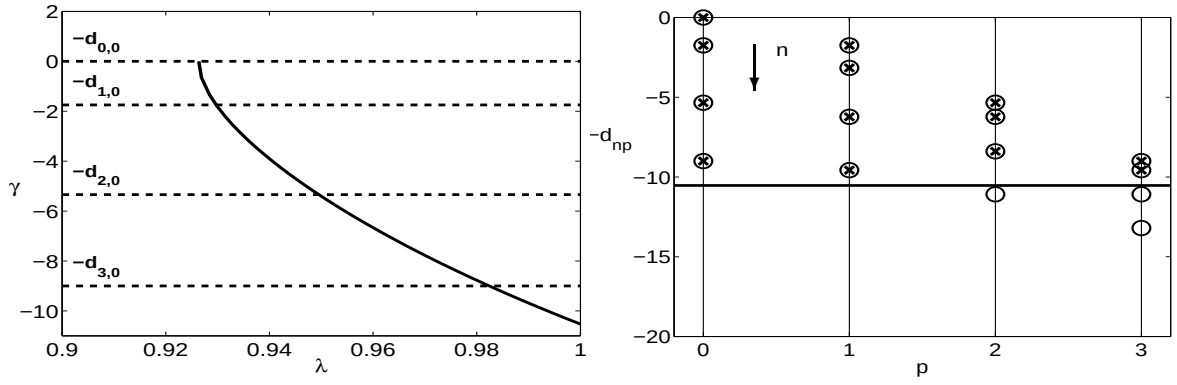

a) *b)*

Figure 4: *Occurrence of bifurcations on the homogeneous $T_F^{(2)}$-branch. Panel a shows function $\lambda \to \gamma(T_F, \lambda)$ along the $T_F^{(2)}$-branch (heavy). The dashed horizontal lines are the values of $-d_{n,p}$. Intersections of γ with $-d_{n,p}$ correspond to a singular Jacobian $\boldsymbol{J}$ and thus to a bifurcation. Panel b shows $-d_{n,p}$ (circles) for $0 \leq n \leq 3$ as a function of the wave number p. Wave number n increases top down (arrow). The crosses mark the values $-d_{n,p}$ above $\gamma_{min} = \gamma(T_F, 1)$ (heavy) and highlight those wave-number pairs (n, p) for which the system undergoes a bifurcation.*

The intersections $\gamma = -d_{n,p}$ correspond to $\zeta_{n,p} = 0$ and thus define the λ-values at which the system undergoes a bifurcation. Figure 4*a* reveals that $\zeta_{n,p} = 0$ occurs for the

case $p = 0$ only for $n = 0, 1, 2, 3$. Furthermore, the monotonic decay of γ with increasing λ causes the intersections – and corresponding bifurcations – to occur in successive order $n = 0, 1, 2, 3$ (from left). With a similar monotonicity argument it follows that the number of intersections decreases monotonically with increasing p. This implies that vanishing coefficients $\zeta_{n,p}$ correspond with those wave numbers $0 \leq n \leq n_{max}(p)$ that satisfy the inequality $d_{n,p} + \gamma_{min} \leq 0$, with $\gamma_{min} = \gamma(T_F, 1)$. Figure 4*b* gives $-d_{n,p}$ (circles) for $0 \leq n \leq 3$ as a function of the wave number p; wave number n increases top down (arrow). The crosses mark the values $-d_{n,p}$ above γ_{min} (heavy) and thus highlight those wave-number pairs (n, p) for which $\zeta_{n,p} = 0$ for some $\lambda \in [0, 1]$ and the system undergoes a bifurcation. It readily follows that here $0 \leq p \leq 3$ and $n_{max}(p) = 3, 3, 2, 1$ for $p = 0, 1, 2, 3$.

Figure 5*a* gives the wave-number pairs (k, ℓ) (stars) for which the present configuration undergoes a bifurcation (Figure 4*b*). The symmetric arrangement of these wave-number pairs w.r.t. the diagonal $k = \ell$ is a manifestation of the square interface (Lemma 1): pairs on the diagonal $k = \ell$ correspond with one single vanishing coefficient $\zeta_{k,\ell} = 0$ (1-mode bifurcation); pairs off the diagonal $k = \ell$ form couples of wave-number pairs ("wave-number groups") $[(k, \ell), (\ell, k)]$ that correspond with two vanishing coefficients $\zeta_{k,\ell} = \zeta_{\ell,k} = 0$ (2-mode bifurcation). The 1-mode and 2-mode bifurcations are indicated by dots and stars, respectively, in Figure 5*b*. The resulting heterogeneous solutions are discussed below.

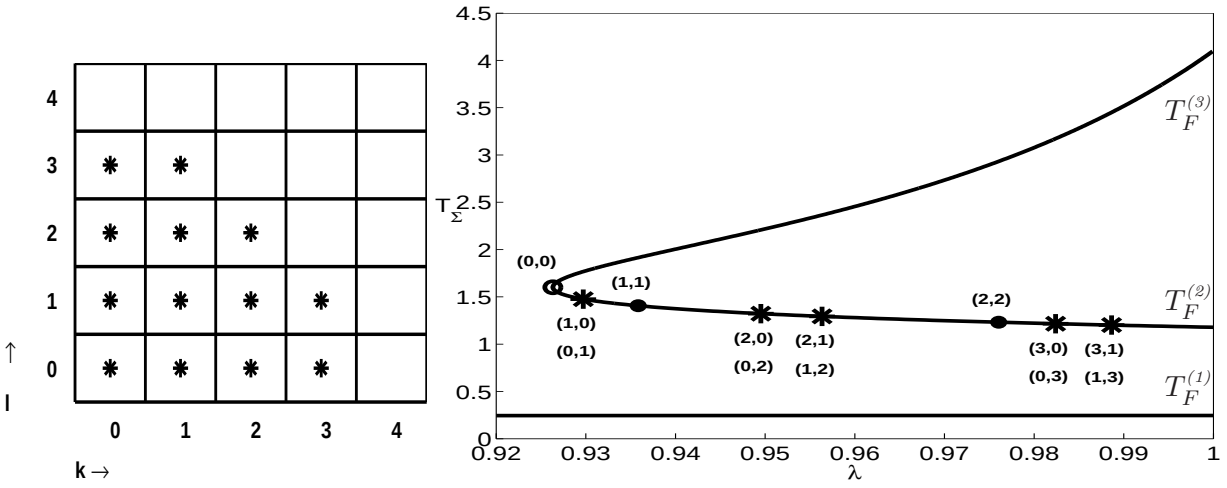

a) *b)*

Figure 5: *Bifurcation behaviour for* $\Lambda = 0.2$, $D_1 = 1$, $D_2 = 0.2$, $\Pi_1 = 4$, $\Pi_2 = 2$ *and* $W = 1$. *Panel a gives the wave-number pairs* (k, ℓ) *(stars) that undergo bifurcations (Figure 4b). Bifurcations on the diagonal* $k = \ell$ *correspond to one single vanishing coefficient* $\zeta_{k,k} = 0$ *(1-mode bifurcation); pairs off the diagonal form wave-number groups* $[(k, \ell), (\ell, k)]$, $k \neq \ell$, *that correspond with two vanishing coefficients* $\zeta_{k,\ell} = \zeta_{\ell,k} = 0$ *(2-mode bifurcation). Panel b gives the bifurcation diagram for the homogeneous solutions in parameter* λ. *The lower branch corresponds with* $T_F^{(1)}$; *the lower and upper legs of the upper branch (connecting at the turning point; circle) correspond with* $T_F^{(2)}$ *and* $T_F^{(3)}$, *respectively.*

5.3 Heterogeneous solutions

The first bifurcation (turning point) on the $T_F^{(2)}$-branch (Figure 5) corresponds with $\zeta_{k,\ell}$ for $k = \ell = 0$ and results in the formation of additional homogeneous solutions. The remaining bifurcations have at least one non-zero wave number and thus involve heterogeneous bifurcation solutions. Two types of such bifurcation points occur here: 1-mode bifurcations ($k = \ell$; dots in Figure 5*b*) and 2-mode bifurcations ($k \neq \ell$; stars in Figure 5*b*). The corresponding heterogeneous solutions are treated below.

1-mode bifurcations For 1-mode bifurcations the null solutions (37) reduce to individual Fourier modes ($m = 1$) and, consequently, heterogeneous solutions of the form

$$T_F(x, y) = T_F^{(2)} + \epsilon \cos(k\pi x) \cos(k\pi y), \quad \epsilon \downarrow 0, \tag{38}$$

emerge ("1-mode bifurcation solution"). This function is an element of the Fourier space $V_{k,k}$. Based on Theorem 1 we conclude that solution branches emerging from the 1-mode bifurcation remain in the Fourier space $V_{k,k}$ (provided no further bifurcation occurs). The bifurcation solution (38) is of the generic form (16) with $\widetilde{T}_{kn,kp} \neq 0$ for $n = p = 1$ and $\widetilde{T}_{kn,kp} = 0$ otherwise. From Theorem 2 it follows that there are corresponding dual-shifted solutions with the self-symmetry properties $T_F(x, y) = T_F^{*,3}(x, y)$, $T_F^* := T_F^{*,1}(x, y) = T_F^{*,2}(x, y)$ and $T_F^* \neq T_F$. Moreover, Lemma 1 implies that in the present case of a square heater each solution has a dual-reflected solution. However, one easily verifies that, since (38) implies $T_F(x, y) = T_F(y, x)$, these dual-reflected solutions coincide with the original ones: $T_F = T_F'$ and $T_F^{*\prime} = T_F^*$. Thus we have a pitchfork bifurcation with a *pair* of solutions (T_F, T_F^*) emerging from the 1-mode bifurcations in Figure 5*b* (dots). Due to Theorem 1 (cf. also Remark 3) *these symmetry properties are preserved along the solution branches*. Figure 6 shows solution T_F for $k = 2$ emerging from the bifurcation (panel *a*). The emergence of its dual-shifted solution T_F^* is similar (not shown). The corresponding final states at $\lambda = 1$ are shown in panels *b* and *c*. Figure 10 (first column) shows the final states ($\lambda = 1$) of the pairs of solutions corresponding with the 1-mode bifurcations, both for $k = 1$ and $k = 2$.

2-mode bifurcations Here the null solutions (37) are spanned by two Fourier modes ($m = 2$) with wave numbers (k, ℓ) and (ℓ, k), $\ell \neq k$ (due to $\zeta_{k,\ell} = \zeta_{\ell,k} = 0$) and yield

$$T_F(x, y) = T_F^{(2)} + \epsilon\big(c_1 \cos(k\pi x) \cos(l\pi y) + c_2 \cos(l\pi x) \cos(k\pi y)\big), \quad \epsilon \downarrow 0, \tag{39}$$

as associated 2-mode bifurcation solution. Such 2-mode bifurcation solutions (39) involve a two-dimensional nullspace spanned by the two associated Fourier modes. This is a fundamental difference with the 2D pool-boiling problem, which admitted only simple vanishing coefficients $\zeta_{k,\ell}$ and thus only one-dimensional nullspaces [1]. The occurrence of higher (than one) dimensional null spaces appears to be an essentially 3D phenomenon.

Multi-dimensional null spaces imply infinite families of bifurcation solutions (39) and thus in principle an infinite family of corresponding branches. However, extensive numerical

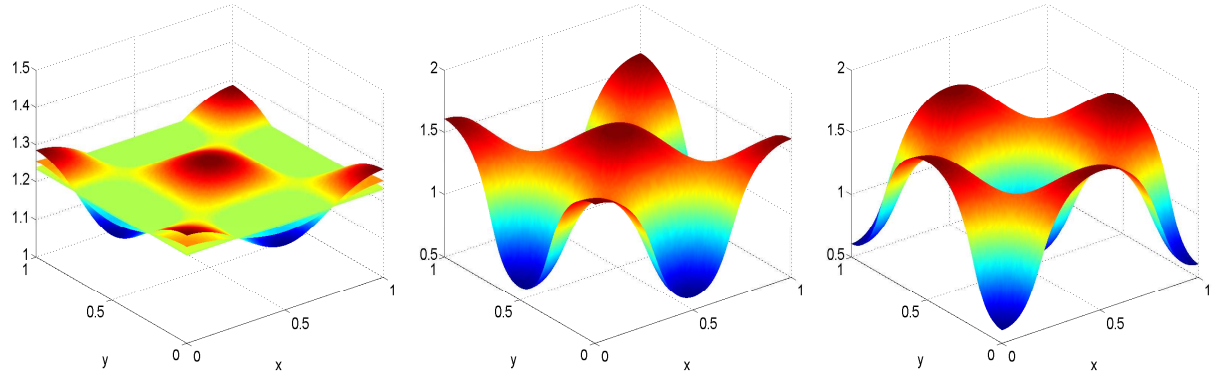

a) T_F: near bifurcation. *b) T_F: final state ($\lambda = 1$).* *c) T_F^*: final state ($\lambda = 1$).*

Figure 6: *Pairwise emergence of heterogeneous solutions from 1-mode bifurcations for the case $k = 2$. Panel a shows T_F for λ just beyond the bifurcation point ($\lambda = 0.97605$); panels b and c show the corresponding final state ($\lambda = 1$) of T_F and its dual-shifted solution T_F^*. The final states are the physically-meaningful steady-state solutions to the boiling problem.*

experiments strongly suggest that (only) the following four classes of 2-mode solutions exist:

$c_1 \neq 0,\ c_2 = 0$ ("quasi 1-mode"; class I), $c_1 = 0,\ c_2 \neq 0$ ("quasi 1-mode"; class II),
$c_1 = c_2 \neq 0$ ("true 2-mode"; class III), $c_1 = -c_2 \neq 0$ ("true 2-mode"; class IV).

The first two classes correspond to 1-mode simplifications of (39); the other two classes to truly 2-mode bifurcation solutions. A theoretical explanation of why (only) these classes of solutions occur is not available yet. The four classes all comprise multiple solutions. The multiplicity is treated in more detail for the first and third classes. The second and fourth classes have properties very similar to the first and third classes, respectively.

Class I: $\mathbf{c_1 \neq 0},\ \mathbf{c_2 = 0}$ In this case the bifurcation solutions (39) reduce to individual Fourier modes and heterogeneous solutions of the form

$$T_F(x,y) = T_F^{(2)} + \epsilon \cos(k\pi x)\cos(\ell\pi y), \quad \epsilon \downarrow 0, \quad k \neq \ell, \tag{40}$$

with $0 \leq k, \ell \leq 3,\ k + \ell \leq 4$, cf. Fig. 5, emerge ("quasi 1-mode bifurcation solution"). The function in (40) is an element of the Fourier space $V_{k,\ell}$. Based on Theorem 1 we conclude that solution branches emerging from such a bifurcation remain in the Fourier space $V_{k,\ell}$ (provided no further bifurcation occurs). We first consider pairs (k,ℓ) with $k \neq 0$ and $\ell \neq 0$. The bifurcation solution (40) is of the generic form (16) with $\widetilde{T}_{0,0} = T_F^{(2)}$, $\widetilde{T}_{kn,\ell p} = \epsilon$ for $n = p = 1$ and $\widetilde{T}_{kn,\ell p} = 0$ otherwise. From Theorem 2 it follows that there are corresponding dual-shifted solutions with the self-symmetry properties $T_F(x,y) = T_F^{*,3}(x,y)$, $T_F^* := T_F^{*,1}(x,y) = T_F^{*,2}(x,y)$ and $T_F^* \neq T_F$. Lemma 1 yields that each of these two solutions has a reflected solution. One easily checks that, as opposed to the case $k = \ell$ considered above, these reflected solutions differ from T_F and T_F^*. Thus we obtain the following cluster of *four* different solutions:

$$T_F \text{ as in (40)}, \quad T_F^* := T_F^{*,1} = T_F^{*,2}, \quad T_F', T_F^{*\prime} \text{ as in Lemma 1.} \tag{41}$$

The symmetry properties are preserved along the solution branches. Thus for $\lambda = 1$ we have a cluster of 4 solutions with the same symmetry properties as in (41). Note that for $T_F = T_F|_{(k,\ell)}$ as in (40) we have $T_F|_{(k,\ell)} = T_F'|_{(\ell,k)}$. From this one easily deduces that the clusters (41) for (k,ℓ) and (ℓ,k) are the same. In Figure 10 these clusters are shown for $(k,\ell) = (2,1)$ (second column) and for $(k,\ell) = (3,1)$ (third column). As noted above, for $(k,\ell) = (1,2)$ and $(k,\ell) = (1,3)$ the clusters are the same as in column 2 and 3, respectively.

We now consider $\ell = 0,\ k \in \{1,2,3\}$. Note that in this case the Fourier mode in (40) is constant in y-direction ("semi-heterogeneous solution"). From Theorem 2 (with $\ell = \infty$) it follows that there are corresponding dual-shifted solutions with the self-symmetry properties $T_F(x,y) = T_F^{*,2}(x,y)$, $T_F^* := T_F^{*,1}(x,y) = T_F^{*,3}(x,y)$ and $T_F^* \neq T_F$. Lemma 1 yields that each of these two solutions has a reflected solution. These reflected solutions differ from T_F and T_F^*. Thus we again obtain a cluster of *four* different solutions:

$$T_F \text{ as in (40)}, \quad T_F^* := T_F^{*,1} = T_F^{*,3}, \quad T_F', T_F^{*\prime} \text{ as in Lemma 1.} \tag{42}$$

The same holds (with $T_F^{*,1}$ and $T_F^{*,2}$ interchanged) for the case $k = 0,\ \ell \in \{1,2,3\}$. The semi-heterogeneous solutions for the case $\ell = 0$ are illustrated in Figure 7

Thus for class I four different heterogeneous solutions as in (41) or (42) exists. By symmetry arguments one can show that for class II *the same* clusters of four solutions as in (41) (for $k \neq 0, \ell \neq 0$), (42) (for $k = 0$) occur.

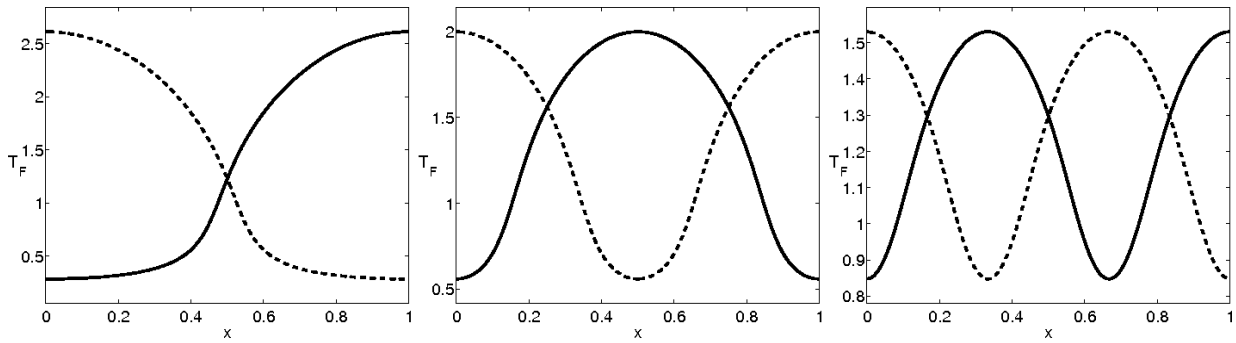

a) (T_F, T_F^*) *for* $(k,\ell) = (1,0)$. *b)* (T_F, T_F^*) *for* $(k,\ell) = (2,0)$. *c)* (T_F, T_F^*) *for* $(k,\ell) = (3,0)$.

Figure 7: *Physically-meaningful* ($\lambda = 1$) *semi-heterogeneous solutions emerging from the quasi 1-mode bifurcation solution. Shown are cross-sections (y fixed) of the temperature profiles* T_F *(solid) and* T_F^* *(dashed) for wave-numbers* $\ell = 0,\ k = 1,2,3$. *The profiles of* T_F' *and* $T_F^{*\prime}$ *are obtained by interchanging* x *and* y.

Class III: $\mathbf{c_1 = c_2 \neq 0}$ In this case the bifurcation solutions (39) are of the form

$$T_F(x,y) = T_F^{(2)} + \epsilon\big(\cos(k\pi x)\cos(\ell\pi y) + \cos(\ell\pi x)\cos(k\pi y)\big), \quad \epsilon \downarrow 0, \quad k \neq \ell, \tag{43}$$

("true 2-mode solution"). Let $q \in \mathbb{N}$ be the maximal common divisor of k and ℓ, i.e., $q \in \mathbb{N}$ is the maximal number such that $k_q := \frac{k}{q} \in \mathbb{N}$ and $\ell_q := \frac{\ell}{q} \in \mathbb{N}$. Note that if $\ell = 0$ ($k = 0$) we have $q = k$ ($q = \ell$) and that if $k\ell \neq 0$ then *not* both k_q and ℓ_q can be even. We first consider the case $\ell = 0$, $k > 0$, for which T_F in (43) is of the form

$$T_F(x,y) = T_F^{(2)} + \epsilon\big(\cos(k\pi x) + \cos(k\pi y)\big). \tag{44}$$

This function is an element of the Fourier space $V_{k,k}$ and has the generic form (16) with

$$\widetilde{T}_{0,0} = T_F^{(2)}, \quad \widetilde{T}_{k,0} = \widetilde{T}_{0,k} = \epsilon \quad \text{and} \quad \widetilde{T}_{kn,kp} = 0 \quad \text{otherwise.} \tag{45}$$

From Theorem 2 it follows that there are dual-shifted solutions $T_F^{*,i}$, $i = 1, 2, 3$. Using (20) and (45) it follows that these dual solutions are different from each other and from T_F. For the dual-reflected solutions we have $T_F' = T_F$, $(T_F^{*,1})' = T_F^{*,2}, (T_F^{*,2})' = T_F^{*,1}, (T_F^{*,3})' = T_F^{*,3}$ and thus these reflections do not yield new solutions. Hence, for $k > 0$, $\ell = 0$ we obtain a cluster of *four* different solutions:

$$T_F \quad \text{as in (44)}, \quad T_F^{*,i}, \ i = 1, 2, 3. \tag{46}$$

Again, these symmetry properties are preserved during the continuation. For $\lambda = 1$ the cluster of four solutions is shown in Figure 11. The case $k = 0$, $\ell > 0$ leads to similar results (with x and y interchanged). The cluster of solutions for $(0, \ell)$ is the same as for $(\ell, 0)$.

For $k > 0$, $\ell > 0$ we have a bifurcating solution of the form

$$T_F(x, y) = T_F^{(2)} + \epsilon\big(\cos(k_q q\pi x)\cos(\ell_q q\pi y) + \cos(\ell_q q\pi x)\cos(k_q q\pi y)\big).$$

This function is an element of the Fourier space $V_{q,q}$. Using Theorem 2, Lemma 1 and symmetry arguments one can show that we have the following multiple solutions:

$$\text{a cluster of four solutions} \ \ T_F, T_F^{*,i}, \ i = 1, 2, 3, \quad \text{if} \ \ k_q + \ell_q \ \ \text{is odd}, \tag{47}$$

$$\text{a cluster of two solutions} \ \ T_F = T_F^{*,3}, T_F^* := T_F^{*,1} = T_F^{*,2} \quad \text{if} \ \ k_q + \ell_q \ \ \text{is even}. \tag{48}$$

(Recall that k_q and ℓ_q cannot both be even). Thus for the case $c_1 = c_2 \neq 0$ the clusters of solutions are given in (46), (47), (48). Note that in the present case study $k_q + l_q$ even (cf. (48)) occurs only for $(k, \ell) = (\ell, k) = (1, 3)$.

For class IV a similar analysis can be performed. It turns out that for $k > 0$, $\ell = 0$ the same cluster of four solutions as in (46) occurs. For $k > 0$, $\ell > 0$ and $k_q + \ell_q$ odd we get the same cluster of four solutions as in (47). For $k_q + \ell_q$ even we obtain a cluster of two solutions that are *different* from the two solutions in (48).

We summarise the results on heterogeneous solutions. The following clusters of heterogeneous solutions have been identified in the present case study:

- Wave numbers (k, k), $k = 1, 2$: one cluster of two 1-mode bifurcation solutions per wave number k (Figure 10; first column).

- Wave numbers (k, ℓ), $k \neq \ell$ with $c_1 = 0$ or $c_2 = 0$: one cluster of four quasi 1-mode bifurcation solutions per wave-number pair (k, ℓ); clusters for (ℓ, k) are identical (Figure 10; second and third columns).

- Wave numbers (k, ℓ), $k \neq \ell$ with $c_{1,2} \neq 0$ and $k = 0$ or $\ell = 0$: one cluster of four true 2-mode bifurcation solutions per (k, ℓ); clusters for (ℓ, k) are identical (Figure 11).

- Wave numbers (k,ℓ), $k \neq \ell$ with $c_{1,2} \neq 0$ and $k\ell > 0$: one cluster of four true 2-mode bifurcation solutions for $k_q + \ell_q$ odd; two clusters each consisting of two true 2-mode bifurcation solutions for $k_q + \ell_q$ even. Here the former and latter occur for $(k,\ell) = (1,2)$ and $(k,\ell) = (1,3)$, respectively. Figure 8 shows one solution ("parent") T_F from each of these clusters. Clusters for (ℓ,k) are again identical.

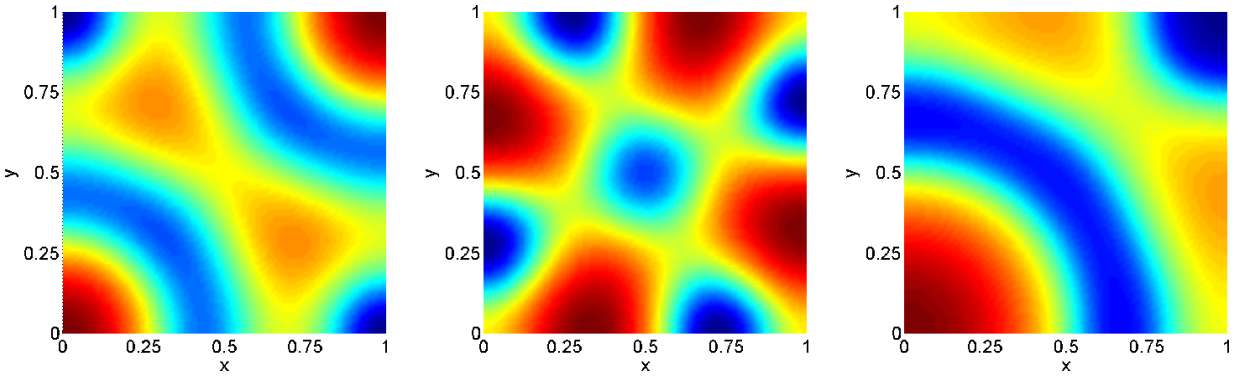

a) $(k,\ell) = (1,3)$*, cluster 1.* *b)* $(k,\ell) = (1,3)$*, cluster 2.* *c)* $(k,\ell) = (1,2)$*.*

Figure 8: *Physically-meaningful* ($\lambda = 1$) *heterogeneous (parent) solutions from 2-mode bifurcation solution clusters. Panels a and b: (parent) solutions of the two true 2-mode clusters for* $(k,\ell) = (1,3)$*. Panel c: (parent) solution of the cluster for* $(k,\ell) = (1,2)$*.*

Figure 9 gives the bifurcation diagram including the full set of solutions found for the case study. For each *cluster* only the branch for the corresponding parent solution T_F is included. (Note that for $(k,\ell) = (1,3)$ we have *two* clusters of true 2-mode solutions and therefore two dashed branches in Figure 9.) For $\lambda = 1$ (the physically-meaningful case study) this amounts to a total of 44 different heterogeneous solutions.

We conclude this section on the case study with the following remarks:

Remark 4 A preliminary stability analysis shows that all heterogeneous solutions as well as the homogeneous solution $T_F^{(2)}$ are unstable in time. Only the homogeneous solutions in the nucleate-boiling ($T_F^{(1)}$) and film-boiling ($T_F^{(3)}$) regimes appear stable. Perturbed heterogeneous solutions converge (for time$\to \infty$) to one of the two homogeneous solutions $T_F^{(1)}$ or $T_F^{(3)}$. However, heterogeneous solutions involving "large" length scales (small wave numbers) can survive for relatively long times. An analysis of this stability issue will be presented in a forthcoming paper.

Remark 5 The above case study revealed that the Jacobian may have two-dimensional nullspaces with corresponding 2-mode bifurcation solutions. However, higher-dimensional nullspaces (i.e. dimension $m > 2$), with corresponding m-mode bifurcation solutions, may occur as well under specific conditions. Flattening the heater studied above ($D_2 = 0.05$ instead of $D_2 = 0.2$) for instance results in the formation of four-dimensional nullspaces and associated 4-mode bifurcation solutions [22]. The corresponding solution structures

exhibit a far greater complexity and richness compared to those found for the case study considered above. This is a further illustration of the intricate multiple solution structure that may be encountered in the 3D boiling problem.

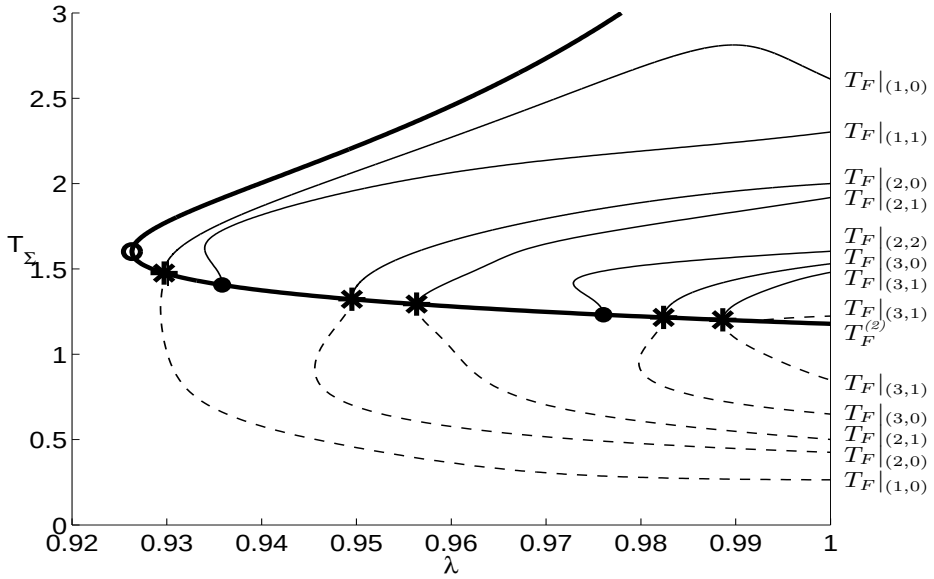

Figure 9: *Bifurcation diagram. Shown are the homogeneous $T_F^{(2)}$-branch (heavy) and heterogeneous branches (solid; dashed) corresponding with a parent solutions from each clusters of solutions. (Subscripts indicate associated wave-number groups.) The solid branches correspond with 1-mode and quasi 1-mode bifurcation solutions; the dashed branches correspond with true 2-mode bifurcation solutions.*

6 Conclusions

In this paper we consider a 3D heat-transfer problem with a nonlinear Neumann boundary condition on part of the boundary as a simple model for 3D pool boiling processes. This model is the same as the one in the 2D pool-boiling problem studied in [1]. The heat flux from the heater to the fluid is modelled by means of a nonlinear functional relation between the local heat flux and the boundary temperature. A key issue is the existence of multiple steady-state solutions with heterogeneous temperature distributions on the fluid-heater interface. The separation-of-variables technique enables analytical reduction of the full 3D problem to a 2D problem for the temperature distribution on the fluid-heater interface (as in (7)). This reduced problem forms the basis of the analysis and is discretised using a Fourier collocation method. This problem has a symmetry property that implies multiplicity of heterogeneous solutions (Theorem 2). These symmetries are direct consequences of the shift-invariance property (21). Multiple (heterogeneous) solutions originate from bifurcations on a branch of homogeneous solutions. *The existence of symmetries (Theorem 2) and the conservation of symmetries during continuation (Theorem 1) are two fundamental*

properties of the model. The steady-state behaviour of the 3D pool-boiling model is studied through a numerical bifurcation analysis of the reduced problem and demonstrates the multiple solution structure by way of a representative case study. Below we outline a few main conclusions from this analysis.

Multiple (heterogeneous) steady-state solutions are found in systems that admit transition boiling modes; systems admitting only nucleate or film boiling allow only one unique and homogeneous solution. Heterogeneous solutions represent temperature distributions that correspond to coexisting nucleate and film boiling regions on the interface. Heterogeneous solutions emerge clusterwise from pitchfork bifurcations on the homogeneous solution branch in the transition regime. The occurrence of (multiple) heterogeneous solutions in the transition regime is consistent with results known from laboratory experiments. This suggests that the proposed model provides an (at least qualitatively) adequate description of 3D pool boiling.

The 3D pool-boiling model behaves to a large extent similar to the 2D model. The 2D and 3D problems share two key properties. Firstly, the shift-invariance property that underlies the fundamental multiplicity in steady-state solutions and secondly, bifurcations undergone by the homogeneous solution in the transition regime are the origin of multiple (heterogeneous) steady-state solutions. There is, however, also a fundamental difference. The 3D system admits bifurcations with multi-dimensional nullspaces; 2D systems, in contrast, admit only one-dimensional nullspaces. This leads to 3D solution structures that have no 2D counterpart. Numerical experiments suggest that the freedom within multi-dimensional nullspaces is restricted in that only specific heterogeneous solutions are allowed to emerge from the corresponding bifurcations. The underlying mechanism for this phenomenon is not yet understood.

Related to current and future research we note the following. Studies on the bifurcation behaviour associated with system parameters other than the artificial nonlinearity parameter considered here are in progress. Preliminary stability studies reveal that steady-state solutions are always unstable, except for a homogeneous solution each in the nucleate and film-boiling regimes. We are currently working on an analysis to explain this stability property. Further issues to be considered in future work may include the effect of different heating methods and stabilisation of pool-boiling processes via active control [8].

Acknowledgment

The presented work has benefitted greatly from the continuation algorithm kindly provided by Robert Grosch, Process Systems Engineering, RWTH Aachen.

References

[1] Speetjens, M., Reusken, A. & Marquardt, W. 2006 Steady-state solutions in a nonlinear pool-boiling model. *IGPM report 256, RWTH Aachen.* Submitted to *Communications in Nonlinear Science and Numerical Simulation*

[2] Thome, J.R. 2003 Boiling. In *Handbook of Heat Transfer* (ed. A. Bejan & A. D. Krause), Wiley & Sons, Hoboken, pp 635-717.

[3] Mudawar, I. 2001 Assessment of High-Heat-Flux Thermal Management Schemes. *IEEE Transactions-CPMT: Components and Packaging Technologies*, **24**, pp. 122-141.

[4] Dhir, V. K. 1998 Boiling Heat Transfer. *Ann. Rev. Fluid Mech.* **30**, 365–401.

[5] Theofanous, T. G.. Tu, J. P., Dinh, A. T. & Dinh, T. N. 2002 The boiling crisis phenomenon. Part I: nucleation and nucleate boiling heat transfer. *Exp. Therm. Fluid Sci.*, **26**, pp. 775–792.

[6] Dhir, V. K. 1991 Nucleate and transition boiling heat transfer. *Int. J. Heat Fluid Flow*, **12**, pp. 290–314.

[7] Auracher, H. & Marquardt, W. 2004 Heat transfer characteristics and mechanisms along entire boiling curves under steady-state and transient conditions. *J. Heat Fluid Flow*, **25**, pp. 223-242.

[8] Auracher, H. & Marquardt, W. 2002 Experimental studies of boiling mechanisms in all boiling regimes under steady-state and transient conditions. *Int. J. Therm. Sci.*, **41**,pp. 586-598.

[9] van Ouwekerk, H. 1972 Burnout in pool boiling. The stability of boiling mechanisms. *Int. J. Heat Mass Transfer*, **15**, pp. 25–33.

[10] Zhukov, S. A., Barelko, V. V. & Merzhanov, A. G. 1980 Wave processes on heat generating surfaces in pool boiling. *Int. J. Heat Mass Transfer*, **24**, pp. 47-55.

[11] Zhukov, S. A. & Barelko, V. V. 1983 Nonuniform steady states of the boiling process in the transition region between the nucleate and film regimes. *Int. J. Heat Mass Transfer*, **26**, pp. 1121-1130.

[12] Gabaraev, B. A., Kovalev, S. A., Molochnikov, Yu. S., Solov'ev, S. L. & Usitakov, S. V. 2001 Rewetting and autowave change of boiling modes. *High Temp.*, **39**, pp. 302-314.

[13] Kovalev, S. A. 1966 An investigation of minimum heat fluxes in pool boiling of water. *Int. J. Heat Mass Transfer*, **9**, pp. 1219-1226.

[14] Kovalev, S. A. & Rybchinskaya, G. B. 1978 Prediction of the stability of pool boiling heat transfer to finite disturbances. *Int. J. Heat Mass Transfer*, **21**, pp. 691-700.

[15] Kovalev, S. A. & Usitakov, S. V. 2003 Analysis of the stability of boiling modes involving the use of stability diagrams. *High Temp.*, **41**, pp. 68-78.

[16] Blum, J., Lüttich, T. & Marquardt, W. 1999 Temperature wave propagation as a route from nucleate to film boiling? In *Proceedings of the Second International Symposium on Two-Phase Flow Modelling and Experimentation, Rome, Vol 1* (ed. G.P. Celata, P. DiMarco & R.K. Shah), Edizioni ETS, Pisa.

[17] Kreyszig, E. 1999 *Advanced Engineering Mathematics*, Wiley, Chichester.

[18] Canuto, C., Hussaini, M. Y., Quarteroni, A. & Zang, T. A. 1987 *Spectral Methods in Fluid Dynamics*. Springer, Berlin.

[19] Gonzalez-Velasco, E. A. 1995 *Fourier Analysis and Boundary Value Problems.* Academic Press, San Diego.

[20] Govaerts, W. J. F 2000 *Numerical Methods for Bifurcations of Dynamical Equilibria*, SIAM, Philadelphia.

[21] Ott, E. 2002 *Chaos in Dynamical Systems.* Cambridge University Press, Cambridge (second edition).

[22] Speetjens, M., Reusken, A. & Marquardt, W. 2006 Steady-state solutions in a three-dimensional nonlinear pool-boiling heat-transfer model. *IGPM-report 263, RWTH Aachen.*

A Proofs of Theorems 1 and 2

Proof of Theorem 1. For $k = \ell = 1$ this is trivial due to the definition of S. We consider $k < \infty,\ \ell < \infty$. The case $k = \infty$ or $\ell = \infty$ (i.e., univariate Fourier series) can be treated similarly and requires only notational modifications. Take $T_F \in V_{k,\ell} \cap S$. Then T_F can be represented as $T_F(x,y) = \sum_{n,p=0}^{\infty} \widetilde{T}_{kn,\ell p} \cos(kn\pi x) \cos(\ell p \pi y / D_1)$ and all Fourier coefficients $\widetilde{T}_{m,r}$ with $m \bmod k \neq 0$ or $r \bmod \ell \neq 0$ are equal to zero. We obtain

$$\begin{aligned}
\mathcal{G}(T_F)(x,y) &= \sum_{n,p=0}^{\infty} d_{n,p} \widetilde{T}_{n,p} \cos(n\pi x) \cos\left(\frac{p\pi y}{D_1}\right) + \alpha(T_F(x,y)) T_F(x,y) - \frac{1}{\Lambda} \\
&= \sum_{n,p=0}^{\infty} d_{kn,\ell p} \widetilde{T}_{kn,\ell p} \cos(kn\pi x) \cos\left(\frac{\ell p\pi y}{D_1}\right) + \alpha(T_F(x,y)) T_F(x,y) - \frac{1}{\Lambda} \\
&=: w_1(x,y) + w_2(x,y) - \frac{1}{\Lambda}.
\end{aligned}$$

From $T_F \in S$ it follows that the series $w_1(x,y) = \sum_{n,p=0}^{\infty} d_{kn,\ell p} \widetilde{T}_{kn,\ell p} \cos(kn\pi x) \cos(\frac{\ell p \pi y}{D_1})$ converges and thus $w_1 \in V_{k,\ell}$. From $T_F \in S$ it also follows that $w_2 = (\alpha \circ T_F) T_F \in V_{1,1}$ and thus w_2 has a convergent double cosine Fourier series. The function T_F is $\frac{2}{k}$-periodic in x and $\frac{2D_1}{\ell}$-periodic in y and thus $w_2 = (\alpha \circ T_F) T_F$ has the same properties. Hence, we have $w_2 \in V_{k,\ell}$. Thus we have $\mathcal{G}(T_F) = w_1 + w_2 - \frac{1}{\Lambda} \in V_{k,\ell}$. □

Proof of Theorem 2. We consider $k < \infty,\ \ell < \infty$. The case $k = \infty$ or $\ell = \infty$ (i.e., univariate Fourier series) can be treated similarly and requires only notational modifications. Note that $T_F \in V_{k,\ell} \cap S$ is even in both variables, $\frac{2}{k}$-periodic in x and $\frac{2D_1}{\ell}$-periodic in y. The function $T_F^{*,i}$ is obtained from T_F by a translation with $\frac{1}{k}$ in x-direction and/or a translation with $\frac{D_1}{\ell}$ in y-direction. Hence, we have $T_F^{*,i} \in V_{k,\ell} \cap S$ for $i = 1, 2, 3$. For $i = 3$

we have

$$T_F(x+1/k, y+D_1/\ell) = \sum_{n,p=0}^{\infty} \widetilde{T}_{kn,\ell p} \cos(kn\pi(x+1/k)) \cos(\ell p\pi(y+D_1/\ell)/D_1)$$
$$= \sum_{n,p=0}^{\infty} (-1)^{n+p} \widetilde{T}_{kn,\ell p} \cos(kn\pi x) \cos(\ell p\pi y/D_1)$$

and thus we obtain the representation in (19). The cases $i = 1, 2$ can be treated similarly to derive the representations in (17) and (18). We now show that $T_F^{*,1} \neq T_F$ holds. The representations of T_F and $T_F^{*,1}$ yield $T_F(x,y) - T_F^{*,1}(x,y) = \sum_{n,p=0}^{\infty}(1 - (-1)^n)\widetilde{T}_{kn,\ell p} \cos(kn\pi x) \cos(\ell p\pi y/D_1)$. Assume that $T_F = T_F^{*,1}$ holds. Then $\widetilde{T}_{kn,\ell p} = 0$ must hold for all odd n and thus we obtain the representation $T_F(x,y) = \sum_{n,p=0}^{\infty} \widetilde{T}_{2kn,\ell p} \cos(2kn\pi x) \cos(\frac{\ell p\pi y}{D_1})$. This implies $T_F \in V_{2k,\ell}$, which contradicts the assumption $T_F \notin V_{k',\ell}$ for $k' > k$. Thus $T_F^{*,1} \neq T_F$ must hold. Similar arguments can be applied to show $T_F^{*,2} \neq T_F$. For $k = \infty$ ($\ell = \infty$) we have $T_F^{*,1} = T_F$, $T_F^{*,2} \neq T_F$ ($T_F^{*,2} = T_F$, $T_F^{*,1} \neq T_F$, respectively). For arbitrary $(x,y) \in \mathbb{R}^2$ we have

$$\begin{aligned}
&\mathcal{G}(T_F^{*,1})(x,y) \\
&= \mathcal{F}^{-1}\big(\mathbf{d} \cdot \mathcal{F}(T_F^{*,1})\big)(x,y) + \alpha(T_F^{*,1}(x,y))T_F^{*,1}(x,y) - \frac{1}{\Lambda} \\
&= \sum_{n,p=0}^{\infty} d_{kn,\ell p}(-1)^n \widetilde{T}_{kn,\ell p} \cos(kn\pi x) \cos\Big(\frac{\ell p\pi y}{D_1}\Big) + \alpha(T_F^{*,1}(x,y))T_F^{*,1}(x,y) - \frac{1}{\Lambda} \\
&= \sum_{n,p=0}^{\infty} d_{kn,\ell p} \widetilde{T}_{kn,\ell p} \cos(kn\pi(x+\frac{1}{k})) \cos\Big(\frac{\ell p\pi y}{D_1}\Big) + \alpha(T_F^{*,1}(x,y))T_F^{*,1}(x,y) - \frac{1}{\Lambda} \\
&= \mathcal{F}^{-1}\big(\mathbf{d} \cdot \mathcal{F}(T_F)\big)(x+\frac{1}{k}, y) + \alpha(T_F(x+\frac{1}{k}, y))T_F(x+\frac{1}{k}, y) - \frac{1}{\Lambda} \\
&= \mathcal{G}(T_F)(x+\frac{1}{k}, y) = 0.
\end{aligned}$$

Hence, $\mathcal{G}(T_F^{*,1}) = 0$ holds. A very similar reasoning can be applied to prove that $\mathcal{G}(T_F^{*,i}) = 0$ holds for $i = 2, 3$ too. □

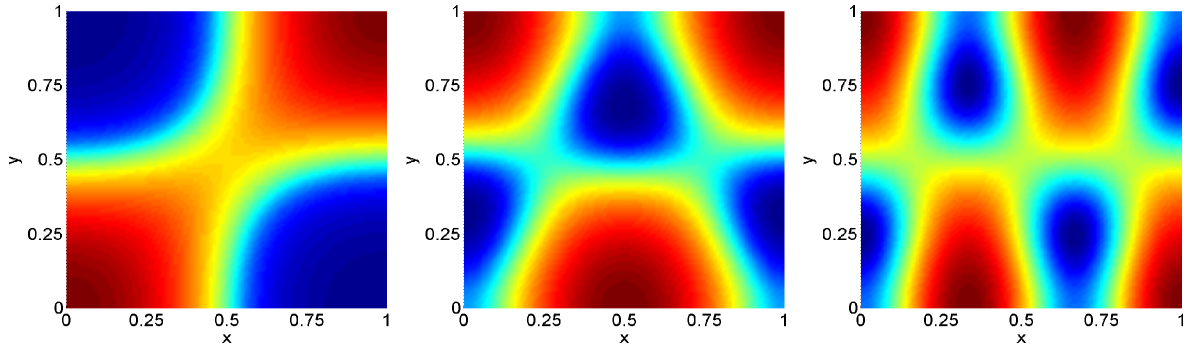

a) T_F *for* $k = 1$.

b) T_F *for* $(k, \ell) = (2, 1)$

c) T_F *for* $(k, \ell) = (3, 1)$

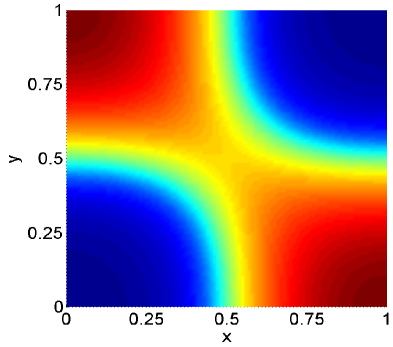

d) T_F^* *for* $k = 1$.

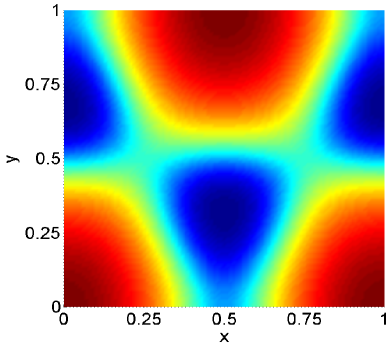

e) T_F^* *for* $(k, \ell) = (2, 1)$.

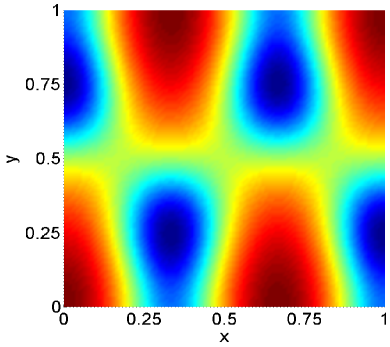

f) T_F^* *for* $(k, \ell) = (3, 1)$.

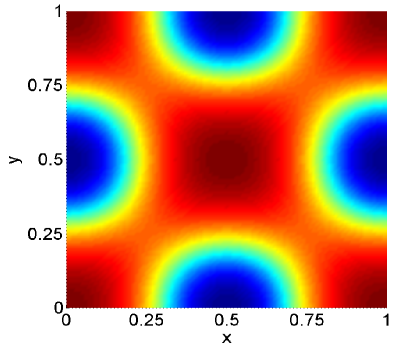

g) T_F *for* $k = 2$.

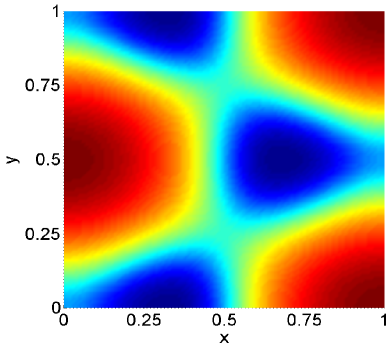

h) T_F' *for* $(k, \ell) = (2, 1)$.

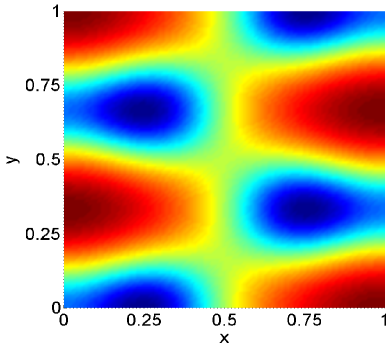

i) T_F' *for* $(k, \ell) = (3, 1)$.

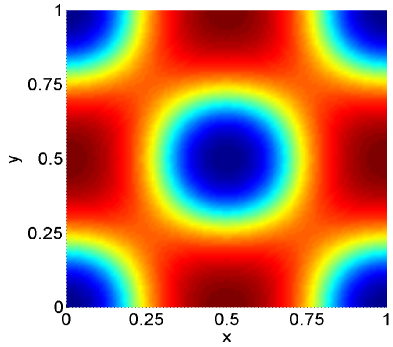

j) T_F^* *for* $k = 2$.

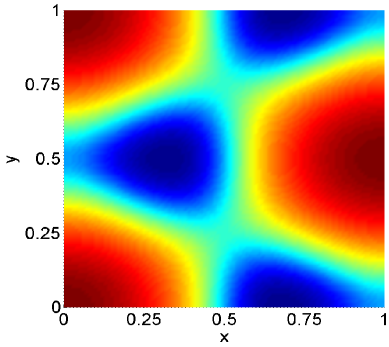

k) $T_F^{*\prime}$ *for* $(k, \ell) = (2, 1)$.

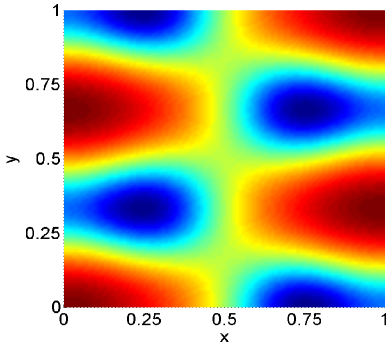

l) $T_F^{*\prime}$ *for* $(k, \ell) = (3, 1)$.

Figure 10: *Physically-meaningful* ($\lambda = 1$) *solutions corresponding with 1-mode bifurcation solutions* (38) *for* $k = 1$ *and* $k = 2$. *The remaining columns give the cluster of 4 solutions* (41) *emerging from quasi 1-mode bifurcation for* $(k, \ell) \in \{(1, 2), (2, 1)\}$ *(second column) and* $(k, \ell) \in \{(1, 3), (3, 1)\}$ *(third column).*

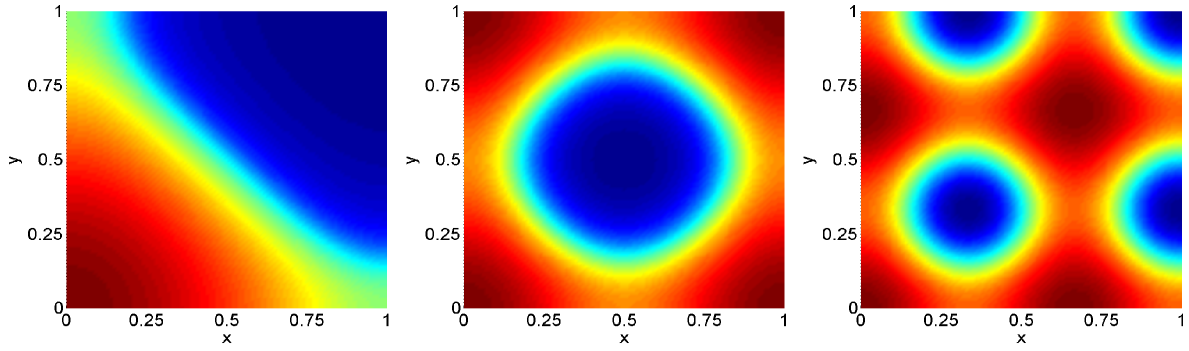

a) T_F *for* $(k,\ell) = (1,0)$. *b)* T_F *for* $(k,\ell) = (2,0)$. *c)* T_F *for* $(k,\ell) = (3,0)$.

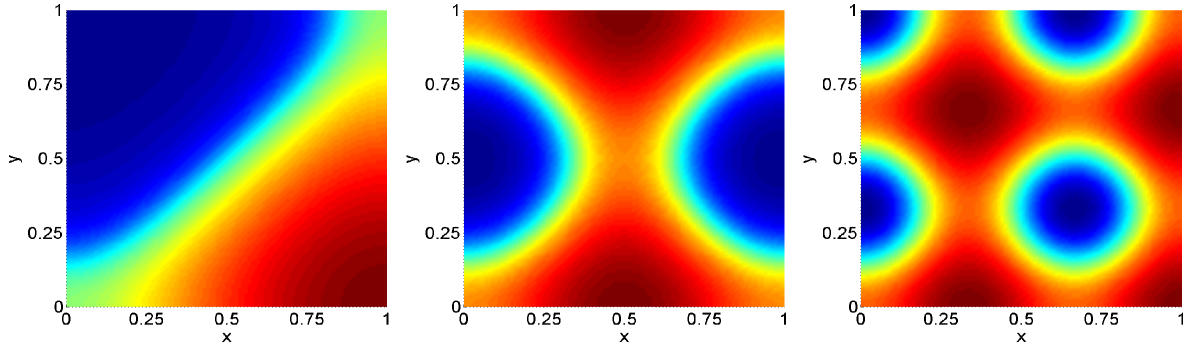

d) $T_F^{*,1}$ *for* $(k,\ell) = (1,0)$. *e)* $T_F^{*,1}$ *for* $(k,\ell) = (2,0)$. *f)* $T_F^{*,1}$ *for* $(k,\ell) = (3,0)$.

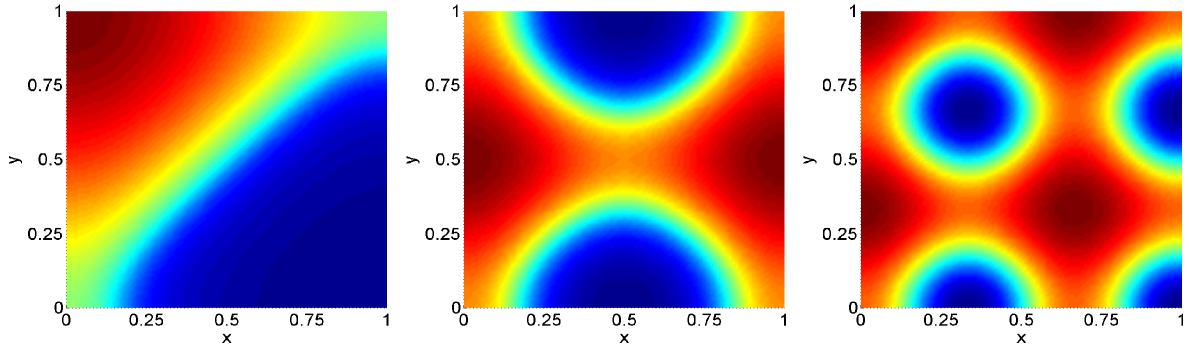

g) $T_F^{*,2}$ *for* $(k,\ell) = (1,0)$. *h)* $T_F^{*,2}$ *for* $(k,\ell) = (2,0)$. *i)* $T_F^{*,2}$ *for* $(k,\ell) = (3,0)$.

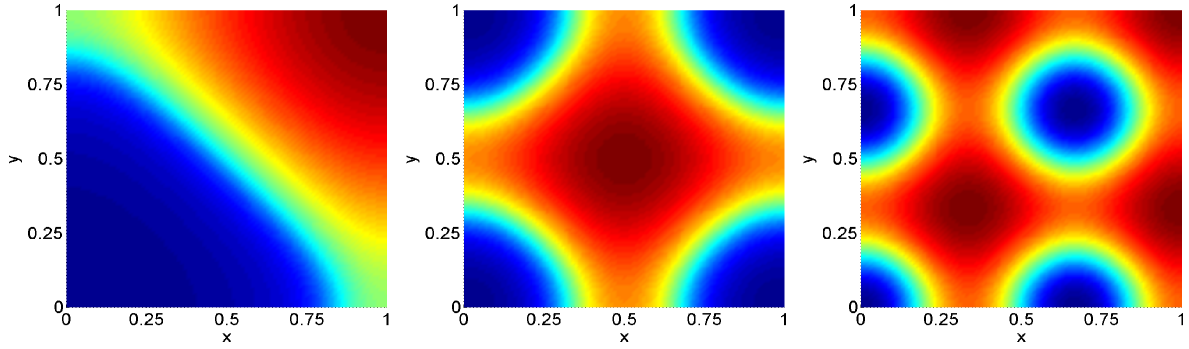

j) $T_F^{*,3}$ *for* $(k,\ell) = (1,0)$. *k)* $T_F^{*,3}$ *for* $(k,\ell) = (2,0)$. *l)* $T_F^{*,3}$ *for* $(k,\ell) = (3,0)$.

Figure 11: *Physically-meaningful* ($\lambda = 1$) *cluster of true 2-mode solutions emerging from the 2-mode bifurcation solutions* (46) *for* $\ell = 0, k = 1, 2, 3$.